Laser Scanning Multiphoton Microscopy

Focusing on Fluorescence Correlation Spectroscopy and Fluorescence Lifetime Imaging for Biomedical Applications

JEEMOL JAMES

UNIVERSITY OF GOTHENBURG

Department of Chemistry and Molecular Biology
University of Gothenburg
2022

DOCTORAL THESIS
Submitted for fulfilment of the requirements for the degree of Doctor of Philosophy in Biophysics

Laser Scanning Multiphoton Microscopy

Focusing on Fluorescence Correlation Spectroscopy and Fluorescence Lifetime Imaging for Biomedical Applications

JEEMOL JAMES

ISBN: 978-91-8009-687-4 [Print]

ISBN: 978-91-8009-688-1 [Pdf]

Available online at: http://hdl.handle.net/2077/70451

Cover Art:

MPM FLIM image a metastasized sentinel lymph node tissue showing the atypical cells and blood vessel obtained from the red channel (580/150 nm) when excited at 780nm. A false-color scale indicating fluorescence lifetime data ranging from 100 – 3000 ps.

Biomedical Photonics Group

Department of Chemistry and Molecular Biology

University of Gothenburg

SE-412 96 Gothenburg

Sweden

Printed by Kompendiet

Gothenburg, Sweden 2022

“Known is a drop and unknown is an ocean”

-Avvaiyar (Tamil female poet, 3rd BC)

To my family and children of my children.

Abstract

Laser scanning multiphoton microscopy (MPM) is considered as a non-invasive technology for three-dimensional imaging of complex biological tissues. The quantitative potential of the MPM is not investigated as much as qualitative imaging. To explore the quantitative aspects, MPM is here combined with fluorescence correlation spectroscopy (FCS) and fluorescence lifetime imaging (FLIM) for different biomedical applications.

The first part of the thesis (papers 1 and 2) emphasizes the importance of validation and optimization of an experimental MPM set up to develop a systematic methodology to combine MPM with FCS utilizing a single-photon counting method. A practical guideline featuring the theoretical and experimental boundaries to implement two-photon excited FCS in the MPM experimental setup is developed in paper 1. Concentration range, numerical aperture of the objective lens, and laser excitation power were found as prime factors to be optimized to study the diffusion time using MPM-FCS. To extend the applicability of MPM-FCS in biological samples, proof of principle was demonstrated by measuring the viscosity of collagen gel from the diffusion time measurements of Rhodamine B in different water glycerol mixtures (Paper 2).

In the final part of the thesis (papers 3 and 4), MPM-FLIM was employed for different biomedical applications. An exploratory study was performed using MPM-FLIM for *ex vivo* investigations in positive and negative sentinel lymph nodes derived from melanoma patients (Paper 3). MPM-FLIM demonstrates the potential to differentiate atypical cells, healthy lymphocytes, and blood vessels in sentinel lymph nodes along with morphological features and fluorescence lifetime data. Two-photon spectral and FLIM characterization of the complex intrinsic cellular fluorophores such as nicotinamide adenine dinucleotide (NADH), flavin adenine dinucleotide (FAD), and keratin in keratinocytes were performed to facilitate the non-invasive imaging of epidermal and dermal tissue cultures *in vitro* (paper 4). This study exposed the importance of keratin signal and should not be neglected when FLIM data is interpreted which needs to be done very carefully in complex biological samples. Taken together, this thesis demonstrates how to adopt MPM in combination with FCS and FLIM highlighting both the methodology development and biomedical applications.

Keywords: Laser scanning multiphoton microscopy, fluorescence correlation spectroscopy, fluorescence lifetime imaging, melanoma metastasis, intrinsic cellular fluorophores.

List of research publications

The work presented in this thesis is based upon four research articles, referred to as Paper 1-4:

Paper 1

Fluorescence correlation spectroscopy combined with multiphoton laser scanning microscopy - a practical guideline

Jeemol James, Jonas Enger, and Marica B. Ericson. *Applied Sciences* 2021, 11(5). https://doi.org/10.3390/app11052122

Paper 2

Validating multiphoton fluorescence correlation spectroscopy as a tool to measure viscosity dependent molecular diffusion

Jeemol James, Jonas Enger, and Marica B. Ericson. [*Unpublished manuscript 2022*]

Paper 3

Report on fluorescence lifetime imaging using multiphoton laser scanning microscopy targeting sentinel lymph node diagnostics

Jeemol James, Despoina Kantere, Jonas Enger, Jan Siarov, Ann Marie Wennberg and Marica B. Ericson. *Journal of Biomed Optics* 2020, 25(7). https://doi.org/10.1117/1.JBO.25.7.071204

Paper 4

Changing the paradigm of interpreting cellular autofluorescence in context of multiphoton fluorescence lifetime imaging focusing on keratinocytes

Monika Malak, Jeemol James, Marica B. Ericson. [*Unpublished manuscript 2022*]

Contribution Report

Contributions by the author (JJ) to the appended papers in this thesis have been the following:

Paper 1: JJ designed and planned the work together with MBE. JJ performed MPM-FCS measurements and analyzed the data with input from MBE. JJ wrote the manuscript together with MBE with input from JE. The corresponding author together with MBE.

Paper 2: JJ designed and planned the work together with MBE. JJ performed MPM-FCS and rheology measurements. Analyzed MPM-FCS data and discussed results with MBE and JE. Wrote the manuscript with input from MBE and JE. The corresponding author together with MBE.

Paper 3: JJ performed MPM-FLIM measurements and analyzed the data with input from DK and MBE. DK designed and planned the clinical study together with MBE. JJ wrote the manuscript together with MBE and DK with input from other authors. The corresponding author together with MBE.

Paper 4: JJ performed, acquired, and processed the MPM-FLIM data and was responsible for the data analysis using SPCImage software and MATLAB. MM designed and performed the biological studies with input from MBE. MPM-FLIM data were analyzed and discussed with MM and MBE. JJ wrote the MPM-FLIM methodology and data analysis part of the manuscript and provided inputs for drafting the manuscript together with MM and MBE.

MBE Marica B Ericson

JE Jonas Enger

DK Despoina Kantere

MM Monika Malak

Publications not included in this thesis

Optimizing Ti:Sapphire laser for quantitative biomedical imaging. Jeemol James, Hanna Thomsen, Dag Hanstorp, Felpe Ademir Aleman Hérnandez, Sebastain Rothe, Jonas Enger, Marica B. Ericson. *Progress in Biomedical Optics and Imaging - Proceedings of SPIE 2018*. 1049824, https://doi.org/10.1117/12.2286732

Spatially confined photoinactivation of bacteria: Towards novel tools for detailed mechanistic studies. Hanna Thomsen, Jeemol James, Anne Farewell, Marica B Ericson. *Progress in Biomedical Optics and Imaging - Proceedings of SPIE*. 2018. 266729, https://doi.org/10.1117/12.2290718

Self-Assembly of Mechanoplasmonic Bacterial Cellulose–Metal Nanoparticle Composites. Olof Eskilson, Stefan B. Lindström, Borja Sepulveda, Mohammad M. Shahjamali, Pau Güell-Grau, Petter Sivlér, Mårten Skog, Christopher Aronsson, Emma M. Björk, Niklas Nyberg, Hazem Khalaf, Torbjörn Bengtsson, Jeemol James, Marica B. Ericson, Erik Martinsson, Robert Selegård, and Daniel Aili. *Advanced Functional Materials* 2020, 30 (40), https://doi.org/10.1002/adfm.202004766

Abbreviations

MPM	Laser scanning multiphoton microscopy
2PE	Two-photon excitation process
FLIM	Fluorescence lifetime imaging microscopy
FCS	Fluorescence correlation spectroscopy
TCSPC	Time correlated single photon counting
NADH	Nicotinamide adenine dinucleotide
FAD	Flavin adenine dinucleotide
Ti:Sa	Titanium Sapphire
FLT	Fluorescence lifetime
NA	Numerical aperture
PMT	Photomultiplier tube
NIR	Near-infrared

Symbols

S_0	Ground energy level
S_1	Excited singlet level
T_1	Excited triplet level
hv	Energy of the absorbed photon
hv'	Energy of the emitted photon
Γ	Rate of fluorescence emission rate
k_{nr}	Rate of non-radiative process
t	Time
τ_D	Lag time
τ_{FLT}	Fluorescence lifetime
τ_D	Translation diffusion time
τ_n	Natural fluorescence lifetime
$C(\mathrm{r}, t)$	Concentration at position r and time t
$F(t)$	Fluorescence intensity as a function of time
$G(\tau_{Lag})$	The normalized autocorrelation function as a function of lag time
$G(0)$	Initial autocorrelation amplitude
D	Diffusion constant
N	Number of particles within the focal volume
η	Viscosity
I	Intensity
χ^2	Chi square

Contents

Chapter 1. Introduction

1. Introduction

The history of microscopes date back to the usage of magnifying glasses in the 15th century and later scientists developed the basic design (Galileo Galilei, Robert Hooke) [1-5] and the theory of image formation in a microscope (Ernst Abbe, August Köhler) [6-8]. The historic invention of lasers, computers, mathematical concepts, and advancements in the electronic industry made revolutionary changes in the field of optical microscopy. Today it is possible to obtain high-resolution three-dimensional images ranging from single cells to organelles with the help of modern optical tools such as confocal [9], multiphoton and super resolution [10] microscopes.

Among the fluorescent microscopes, the invention of laser scanning multiphoton microscopy (MPM) by W Denk and his colleagues in 1990 was a breakthrough in the field of biomedical imaging [11]. MPM has been greatly explored in generating three-dimensional images of optically dense and light scattering biological samples, especially human skin [12-14]. MPM is capable to penetrate the tissues deeper as the two-photon excitation process (2PE) utilizes near-infrared range light. Another advantage is, the optical sectioning without pinhole aperture as compared to the confocal microscopes. Due to these reasons, MPM has been applied to image human skin tissues to investigate primary melanoma, drug delivery studies, and many more applications [14-17].

However, the outputs of many of these studies are microscopic images providing qualitative information such as cell structure and morphology of skin where quantitative data is missing. In order to obtain quantitative information, MPM can be combined with advanced fluorescence techniques such as fluorescence lifetime imaging microscopy (FLIM) and fluorescence correlation spectroscopy (FCS) [18-20]. FLIM provides lifetime information of the fluorophores from each pixel in an image with a time resolution down to a few hundred picoseconds which can be used to map the local environment inside biological systems [21, 22]. In FCS, molecules in a small focal volume of around a few femtoliters are excited and fluctuation in fluorescence intensity is recorded and correlated. FCS can be employed to study molecular interactions as fluctuations in fluorescence intensity happen due to rotation, diffusion and intersystem crossing [23-27].

The primary aim of this thesis is to combine MPM with FCS and FLIM utilizing the single-photon counting detection method for different biomedical applications. In research, the development of a robust methodology is highly important to further extend the studies. Hence,

optimization and validation of an experimental MPM setup were performed in parallel with the biomedical applications. Paper 1 demonstrates a systematic methodology to combine MPM with FCS by developing a practical guideline featuring the theoretical and experimental conditions. Paper 2 shows the proof of principle of linear relationship between viscosity and diffusion time obtained from MPM-FCS data of rhodamine B in water glycerol mixtures. In papers 3 and 4, MPM-FLIM was applied for answering different biomedical questions. One is, melanoma metastasis in human sentinel lymph nodes obtained from melanoma patients are studied. This was done to investigate the potential of MPM-FLIM to be developed as a non-invasive optical tool to diagnose melanoma metastasis to improve medical treatment. Two-photon characterization of complex intrinsic cellular fluorophores is crucial to employ MPM-FLIM for *in vitro* skin culture studies targeting applications such as organ on a chip [28, 29]. Two-photon spectral and FLIM characterization of intrinsic cellular fluorophores like nicotinamide adenine dinucleotide (NADH), flavin adenine dinucleotide (FAD), and keratin in cellular monolayers of keratinocytes and fibroblasts are performed to target the non-invasive imaging of epidermal tissue cultures *in vitro* (paper 4).

The thesis is structured as follows: chapter 2 introduces the aim and specific objectives addressed in this thesis. Chapter 3 helps to understand the basic background and theory related to fluorescence, two-photon excitation, and MPM. It also explains the theory of FCS, FLIM, and the fundamental principle of the single-photon counting method. In chapter 4, the different biomedical applications searched for in this thesis are featured. In chapter 5, the demonstration of the experimental MPM setup and how it is adopted for FCS and FLIM with single-photon counting method is presented. In chapter 6, the highlighted results from papers 1-4 are discussed. Finally, chapter 7 contains the conclusion from the main findings and the future outlook on how to extend this work to continue the wheel of research.

Chapter 2. Aim and Specific Objectives

2. Aim and Specific Objectives

The overall aim of this thesis is to adopt MPM focusing on fluorescence techniques as FCS and FLIM applied for different biomedical applications. One part of this study is the development of a systematic methodology for MPM together with FLIM and FCS. This is achieved by validating and optimizing an experimental MPM setup to enable FLIM and FCS functionalities. In parallel to this, the developed methodology is applied for solving relevant biomedical questions. A better understanding of the methodology is crucial to obtain fundamental knowledge to differentiate the strengths and weaknesses of the MPM experimental set-up so that FCS and FLIM can be applied to solve appropriate biomedical problems.

The specific targeted scientific questions for each project performed during the Ph.D. period are listed below.

- What are the experimental constraints when performing FCS considering concentration range, selection of objective lens, excitation laser power, and appropriate data analysis? (**Paper 1).**
- How MPM-FCS can be applied to measure diffusion as a function of viscosity based on the FCS measurements performed in different water glycerol mixtures? (**Paper 2**).
- What is the potential of MPM-FLIM to diagnose melanoma metastasis in sentinel lymph nodes extracted from melanoma patients? (**Paper 3**).
- How to perform the characterization of intrinsic cellular fluorescence in keratinocytes using 2PE and MPM-FLIM? (**Paper 4**).

Chapter 3. Background and Theory

3. Background and Theory

3.1. Fluorescence

The following section describes the basic principles of fluorescence and it is inspired from the textbook 'Principles of fluorescence spectroscopy' by Joseph Raymond Lakowicz [30]. Different processes associated with light-matter interaction are visualized in the Jablonski diagram (Figure 1). The light source can be a lamp or laser and the molecules capable of absorbing and emitting photons are known as fluorophores. As seen in the figure, an electron from the ground state (S_0) in the molecule is excited to the higher singlet energy level (S_1 or S_2) when a photon is absorbed by the fluorophore. For this event to happen, the energy of the absorbed photon should be equal to or greater than the minimum energy difference between ground state (S_0) and the higher excited energy level (S_1).

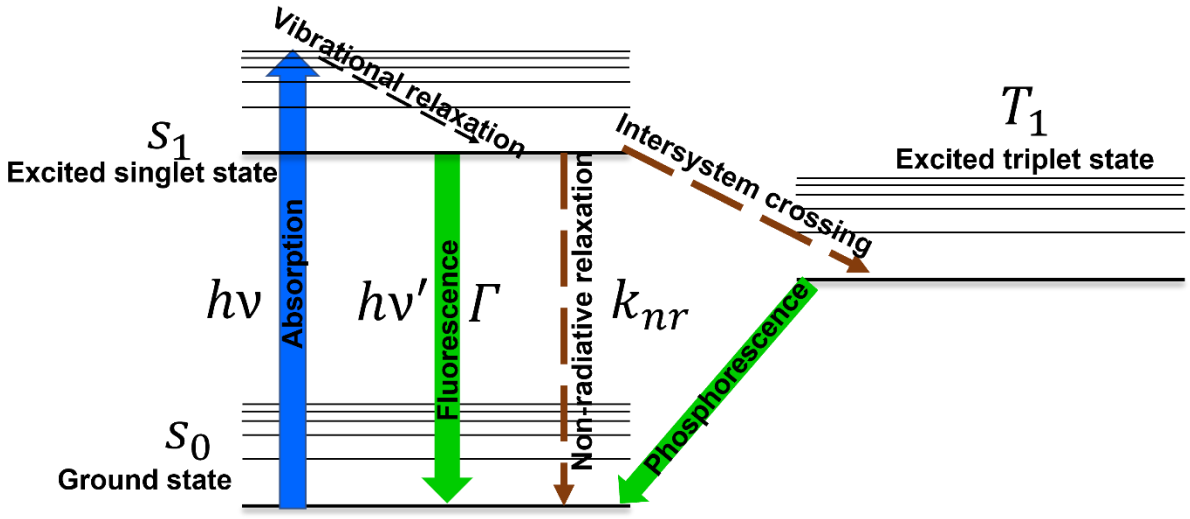

***Figure 1**. Jablonski diagram demonstrating the basic principle of fluorescence as inspired by Lakowicz et al [30]. S_0 , S_1 represent the ground state and the excited state respectively and T_1 shows the excited triplet state. $h\nu$ is excitation photon and $h\nu'$ shows the emitted photon. Dashed arrows represent vibrational relaxation. Γ is the rate of fluorescence emission rate and k_{nr} is the rate of the non-radiative process.*

The excited molecules can return to the lowest vibrational level of S_1 by various radiative or non-radiative processes. In the non-radiative relaxation pathway, by interaction with surroundings and dissipating heat the molecules losses energy and returns to the lowest ground state S_0. One of the radiative processes is known as fluorescence in which molecules return to the S_0 ground state from the lowest vibrational level of S_1 by emitting a photon. This process

happens on the time scale of 10^{-9} sec (fluorescence lifetime). In fluorescence, the emission happens at a longer wavelength compared to excitation as the energy of the emitted photon is lower due to vibrational relaxations and internal conversions. This difference in the emission wavelength is a characteristic property of fluorescence referred to as Stokes shift. There are other pathways for the excited electrons to reach the ground state. The excited electrons in the S_1 singlet excited state can go through a spin conversion to the triplet excited state (T_1) by a process known as an intersystem crossing. Phosphorescence happens when photon emission occurs from T_1 to S_0. Since singlet to triplet transition is forbidden the phosphorescence decay to S_0 is slow, related to fluorescence. The time scale of phosphorescence is in the order of 10^{-3} sec.

Fluorescence lifetime is defined by the average time the molecule stays in the excited state before returning to the S_0 ground state. The fluorescence lifetime can be expressed as

$$\tau_{FLT} = \frac{1}{\Gamma + k_{nr}} \quad (1)$$

where Γ is the rate of fluorescence emission rate and k_{nr} is the rate of all possible non-radiative decay processes. In the absence of non-radiative decay, the fluorescence lifetime τ_{FLT} known as natural lifetime, τ_n, and is given by,

$$\tau_n = \frac{1}{\Gamma}. \quad (2)$$

The natural fluorescence lifetime of a fluorophore is constant at a given solvent. Thus, it is evident that fluorescence lifetime is primarily influenced by the factors that affect both radiative and nonradiative pathways. In this thesis, fluorescence is the key phenomenon that is used in all the studies presented. The process of analyzing the fluorescence signal differs from papers 1-4. In papers 1 and 2, fluctuations in fluorescence intensity are studied to obtain FCS data. Whereas papers 3 and 4 deal with fluorescence lifetime for MPM-FLIM studies.

3.2. Multiphoton microscopy based on two-photon excitation

Multiphoton microscopy (MPM) is an advanced laser scanning microscopy technique that uses a laser beam to excite the fluorophores by the process of multiphoton excitation instead of the conventional one-photon process as in other confocal laser scanning microscopes [9, 31]. Two-photon excitation is a specific case of the multiphoton process. The core of this thesis is multiphoton microscopy which is based on two-photon excitation. The idea of two-photon excitation was first predicted by Maria Goeppert Mayer in her Ph.D. thesis in 1930 [32] but it

was not implemented in microscopy until the invention of pulsed lasers in 1990 [11]. Since then, MPM became popular among biomedical researchers [12, 13, 18, 33, 34].

Figure 2 demonstrates the differences in the optical setup of confocal microscopy and multiphoton microscopy along with the Jablonski diagram comparing the one-photon and two-photon excitation processes. The fluorescence can also happen by the absorption of two or more photons simultaneously rather than absorbing one photon at a time as shown in figure 2. As seen in the figure, simultaneous two-photon absorption occurs via a virtual state if the photon flux density is high enough. This is made possible with high-intensity laser pulses with short duration (~100 fs) which provides high peak power (~200 kW) and low average power (~1 W). As multiphoton excitation involves two or more photons, it is a non-linear process and probability for this event is a function of quadratic power of excitation intensity.

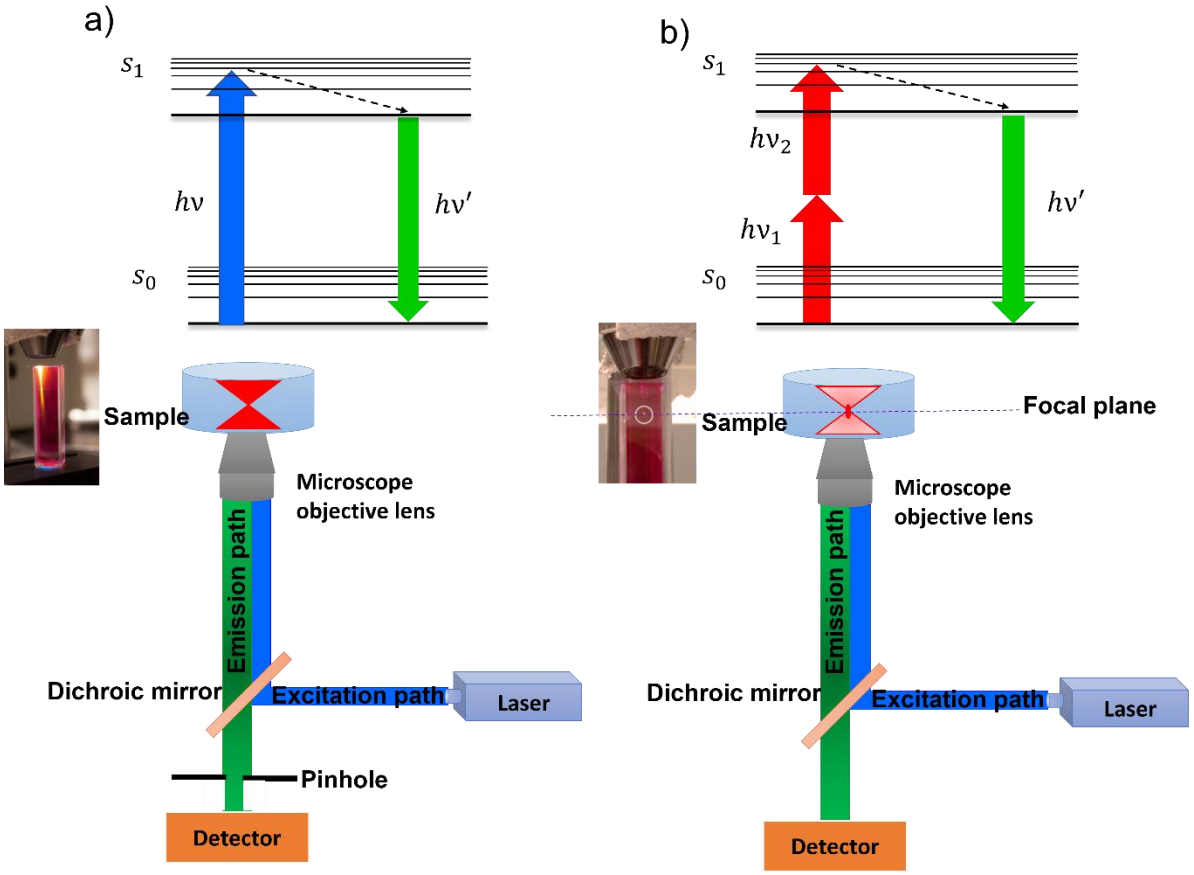

Figure 2. *Comparison of a) one-photon and b) two-photon excitation along with the optical setup of confocal (b) and multiphoton microscopy (b).* S_0 , S_1 *represent the ground state and the excited state.* $h\nu_1$ *and* $h\nu_2$ *are excitation photons for two-photon excitation where* $h\nu$ *is for one-photon excitation and* $h\nu'$ *shows the emitted photon. Dashed arrows represent vibrational relaxation. Photo credits-Johan Borglin.*

Multiphoton excitation happens only at the focal plane as shown in figure 2, whereas all the molecules in the focal volume are excited in confocal microscopy via the one-photon process. Due to the nonlinear property of two-photon excitation, MPM possesses inherent optical sectioning ability without the need of a pinhole as in the case of confocal microscopy (fig 2.a). Also, multiphoton excitation requires photons of lower energy usually coming under near infra-red region (NIR) which is optimum for imaging biological samples as they penetrate deep inside the sample; because of these reasons, MPM is widely utilized for imaging biological specimens [33-37]. Other non-linear effects such as second harmonic generation and three-photon excitations can be utilized by using MPM for various biomedical applications [18, 38, 39].

The experimental set-up of MPM used in this thesis is described in the method section. This MPM set-up equipped with a time-correlated single-photon counting (TCSPC) detector modules were validated and adopted for FLIM and FCS for different applications and they are described in the following sections.

3.3. Fluorescence lifetime imaging microscopy (FLIM)

Fluorescence lifetime imaging microscopy (FLIM) is a quantitative fluorescence technique that generates images based on the excited-state lifetime of the fluorophore rather than the fluorescence intensity. The fluorescence lifetime signal is mainly independent of the intensity of excitation and concentration. Rather it is depending on the microenvironment of the fluorophores such as pH, ion or oxygen concentration, molecular binding [21, 22]. Thus, combining FLIM with MPM becomes interesting as this technique can be employed to map the fluorophores within complex biological samples. A considerable amount of literature has been published on MPM-FLIM employed to probe the metabolic state of malignant biological tissues and human skin [40-42]. The metabolic imaging is executed by taking advantage of the changes in the autofluorescence lifetime originating from a free and bound form of nicotinamide adenine dinucleotide (NADH) and flavin adenine dinucleotide (FAD) [43, 44]. FLIM also has been applied for other applications like pH sensing in living cells [44], protein interaction, and drug delivery studies using Föster resonance energy transfer [45, 46].

Fluorescence lifetime can be measured by either frequency domain or time domain method [22, 47]. Intensity-modulated light such as sine wave modulation is used to excite the fluorophore in the frequency domain method. In this thesis, the time domain method by the

3.Background and Theory

TCSPC is adopted for fluorescence lifetime measurements and it is described in the method section.

In the time domain method, the fluorophore is excited with a pulsed light preferably laser pulse shorter than the fluorescence lifetime τ_{FLT}. Due to the pulsed light excitation the excited state depopulates as follows,

$$\frac{dn(t)}{dt} = (\Gamma + k_{nr})\, n(t) \qquad 3$$

where Γ is the rate of fluorescence emission rate, k_{nr} is the rate of all possible non-radiative decay processes and $n(t)$ is the number of molecules in the excited state at time t after the excitation. Since the fluorescence emission is a random event, the excited state population, and time-dependent fluorescence intensity function $I(t)$ follows an exponential decay,

$$I(t) = I_0 \exp(t|\tau_{FLT}) \qquad 4$$

where $I_0$is the initial intensity. However, in most of the cases the biological samples contain many fluorophores having different lifetime values. In some cases, an intrinsic fluorophore can have a different fluorescence lifetime resulting from binding to a protein, enzyme, or other processes inside the cellular environment. **Figure 3** shows fast (τ_1) and slow (τ_2) components of a fluorescence decay function.

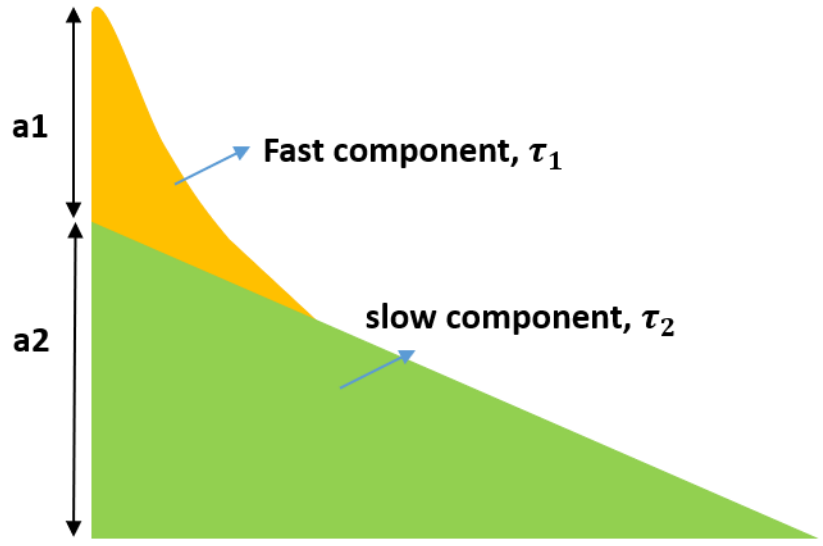

Figure 3. *Fluorescence decay function showing fast (τ_1) and slow (τ_2) lifetime components.*

The fluorescence decay function can be modeled as a multiexponential decay,

$$I(t) = \sum_i \alpha_i \exp(t|\tau_i) \quad 5$$

where α is the pre-exponential factor of the decay fluorescence function of each species in the sample or from different forms of the fluorophore. The fluorescence lifetime becomes the average of the fluorescence lifetime contribution from each species in the sample as follows,

$$\tau_{FLT} = \sum_i \alpha_i \tau_i \quad 6$$

One such example is the fluorescence lifetime of the free and bound form of NADH [43, 44]. More details about implementing FLIM together with MPM is described in the method section and it is explored in paper 3 and 4.

3.4. Time correlated single photon counting (TCSPC)

Time correlated single photon counting (TCSPC) detection method is used throughout this work for all the data acquisition associated with FLIM and FCS studies and the general principle is presented here. TCSPC is a digital time-resolved detection method and single photons from a periodic light signal preferably originating from a high repetitive rate laser are detected [48-51]. The detector signal consists of low intensity at a high repetitive rate and due to this reason, the probability to find a single photon from an excitation pulse is too low. Therefore, the second photons from the excitation pulse are neglected. A histogram of photon arrival time with respect to the excitation pulse is constructed. A schematic diagram explaining the general principle of the TCSPC method is shown in **Figure 4**. As seen in the figure, single photons are detected in each signal period but there are signal periods without individual photons, like in period 3. The photons are detected along with the time of arrival in connection to the excitation pulse in each signal period and this procedure is repeated. The arrival time of the photons is registered in the computer memory. After collecting photons from the signal period, a histogram showing the distribution of photon arrival time is constructed. The histogram of the photon detection time provides the optical waveform of the emission signal.

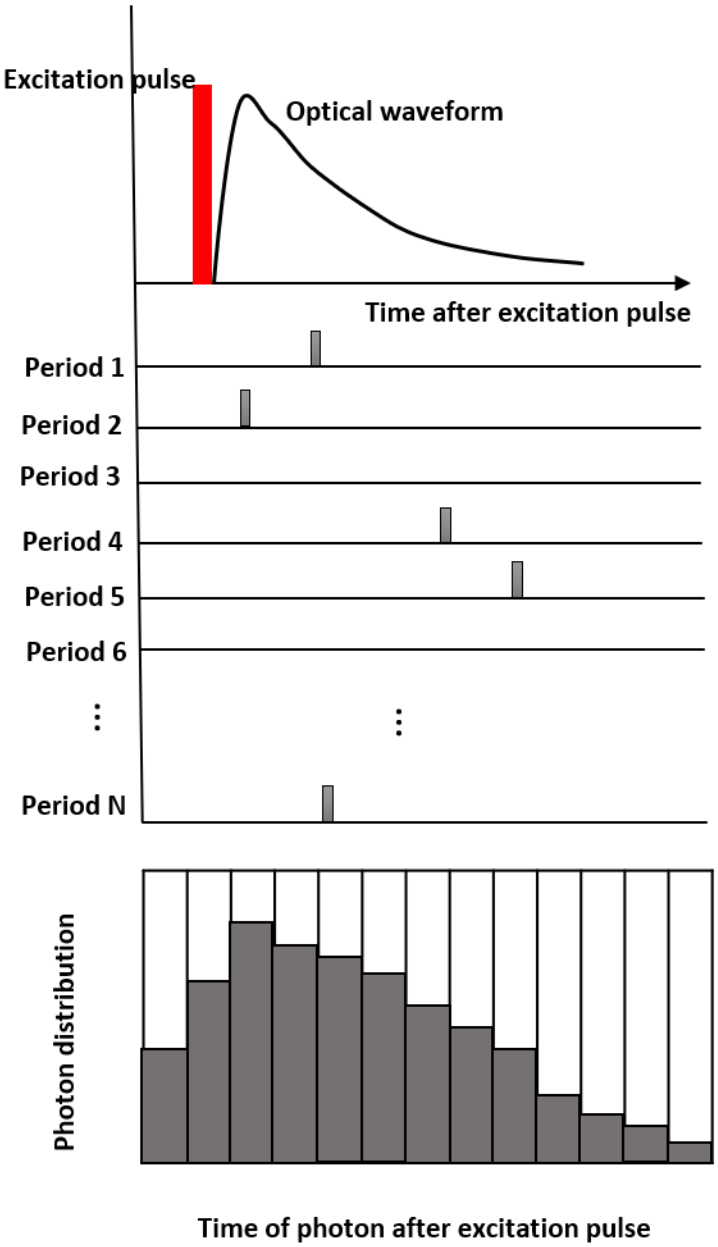

Figure 4. *Schematic of the general principle of TCSPC method, modified from [52].*

TCSPC detection method provides high time resolution as compared to other analog techniques. Because of the transit time spread of the detector and not by the width of the output pulse of the detector [52]. Apart from that, TCSPC has a high signal-to-noise ratio, gain stability, count rates in the range of MHz, and data acquisition time as minimum as a few milliseconds. In TCSPC, it is possible to record the signals from many detectors simultaneously and can be combined with fast laser scanning microscopy like MPM. It is possible to obtain fluorescence lifetime and fluorescence correlation data simultaneously using the TCSPC

technique and it is presented in papers 1-4. The architecture of a TCSPC setup for adopting MPM for both FLIM and FCS is discussed in the method section.

3.5. Fluorescence correlation spectroscopy (FCS)

Fluorescence correlation spectroscopy (FCS) has been an interest of research since the first publication of seminal papers by Elson and Magde published in the 1970s for investigating chemical kinetics and rates [23, 53]. The general principle of FCS is shown in figure 5.a. As seen in the figure, in FCS, molecules in a small volume preferably femtoliters are excited by a light source. The fluctuations in fluorescence intensity when the molecules diffuse in and out of the excitation volume are recorded and correlated. The fluctuations in fluorescence intensity can be due to rotation, diffusion, and intersystem crossing. Theoretical and experimental studies proved FCS as a probe to molecular dynamics to measure these parameters [23-27]. The combination of FCS with both confocal and MPM demonstrated the potential of FCS for studying molecular dynamics in solutions and other biological samples [20, 54-57].

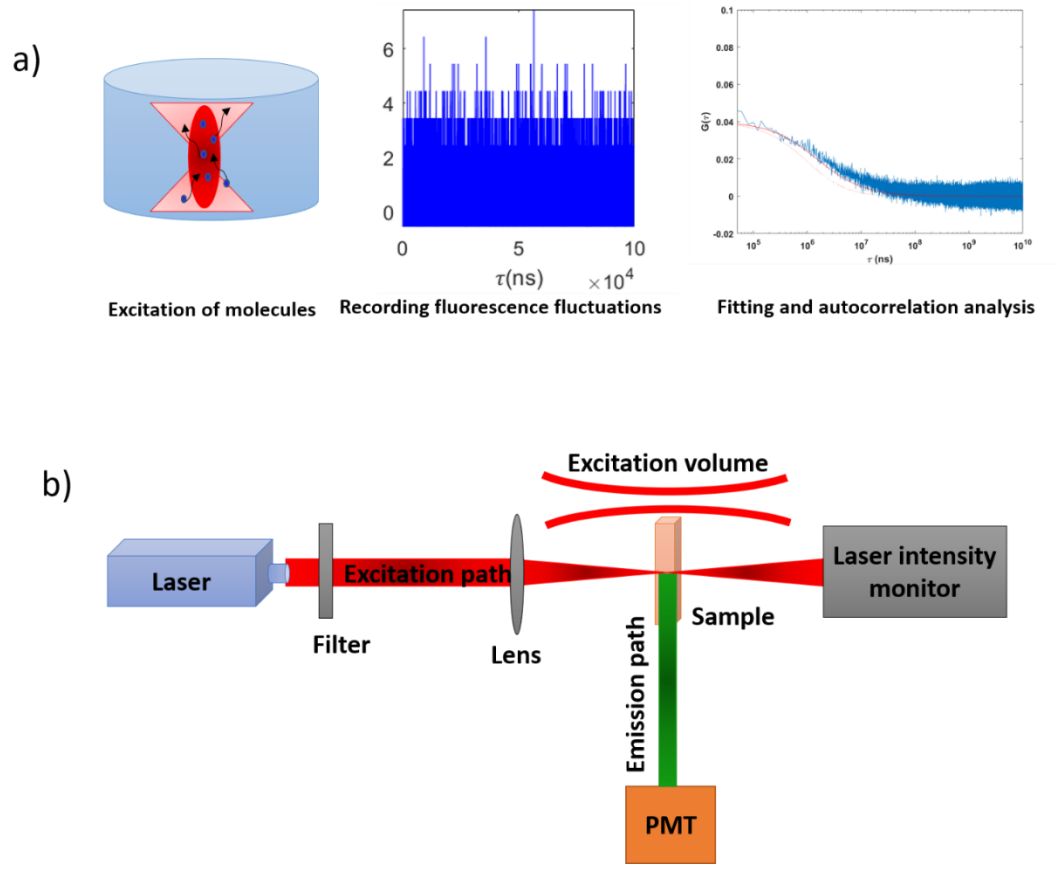

Figure 5. *Schematic diagram of the fundamental principle of FCS (b) and experiment experimental setup used to explain the theory of FCS as adopted from the original paper by Magde et al 1974* [23, 53].

3.Background and Theory

The mathematical explanation of FCS as described by Magde and Elson in their paper published in 1974 [23, 53]. In their work, the FCS experiment was implemented by an Argon laser into a cuvette with a fluorescent solution as shown in figure 5.b. As a result of this, an elongated excitation volume is created instead of tightly focused detection volume by the high numerical aperture of objective lenses. However, the fundamental concepts and theory explained by Magde and Elson will be the same for MPM-FCS.

According to their method, the rate of decay of spontaneous concentration fluctuations of fluorophores in the detection volume conveys information related to molecular diffusion as well as chemical reaction kinetics. This is due to the fact that, at equilibrium the local concentration of molecules fluctuates constantly because of thermodynamic processes. As stated by Magde and Elson "Observation of these spontaneous fluctuations can yield a complete kinetic description of the system equivalent to that obtained by conventional means". This means that we can interpret microscopically defined spontaneous fluctuations at equilibrium using the same theory as applied to at the macroscopic level in non-equilibrium systems.

According to their theory, the local concentration of a chemical compound at a location (**r**) and a given time (*t*) in the sample can be defined as $C(\mathbf{r}, t)$. Elson and Magde (1974) developed the theory using two different chemical components, j and i respectively, to interpret the context of chemical kinetics. To reduce the complexity, here diffusion of one single chemical component is described. The thermodynamic mean concentration is given by the macroscopic equilibrium concentration is independent of position and time,

$$\langle C(\mathbf{r}, t)\rangle = \bar{C} \qquad 7$$

where ⟨ ⟩ denotes ensemble average. Thus, deviation from equilibrium concentration is defined as

$$C(\mathbf{r}, t) = C(\mathbf{r}, t) - \bar{C}. \qquad 8$$

The concentration correlation function at location **r** can be defined as,

$$\phi(\tau_{Lag}) = \langle \delta C(t) \delta C\big(t + \tau_{Lag}\big)\rangle \qquad 9$$

where the variable τ_{Lag}[1], also called the lag-time, denotes a time different from the absolute time *t*.

Using the same theory as proposed by Madge and Elson for the fluorescence fluctuations that happen in the excitation volume created by a pulsed laser, the fluctuations in fluorescence intensity $\delta F(t)$ around the mean value $\langle F(t)\rangle$ is given by

$$\delta F(t) = F(t) - \langle F(t)\rangle, \qquad 10$$

where $F(t)$ is fluorescence intensity. The normalized autocorrelation function $G(\tau_{Lag})$ of fluorescence intensity $F(t)$ at a time t and later time $F(t + \tau_{Lag})$ is given by

$$G(\tau_{Lag}) = \frac{\langle \delta F(t)\, \delta F(t + \tau_{Lag})\rangle}{\langle F(t)\rangle^2}. \qquad 11$$

In TCSPC, the arrival time of the photons (micro time) and time from the start of the experiment (macro time) are saved. The fluorescence decay curve is constructed from the micro time and the FCS curve is obtained by correlating the macro time[49, 58]. Thus, autocorrelation function becomes,

$$G(\tau_{Lag}) = \sum N(t)N(t + \tau_{Lag}) \qquad 12$$

where $N(t)$ is photon count Vs time vector. To extract diffusion information from $G(\tau_{Lag})$ binning of *N(t)* has to be performed. Instead of commonly used multi-tau algorithms, a linear tau algorithm suggested by a previous report has been used in this thesis for data analysis [48]. Multi-tau algorithms are used during the data acquisition process as instant guidance due to the higher speed [59]. In the linear-tau algorithm, different time binning is tested to obtain reliable FCS data. The count vs time vector *N(t)* changes from binary values and the photon count starts to fluctuate around a mean photon value when the time binning is increased. This is explained in detail in the methods section (section 5.2). Thus, the autocorrelation function for the time binned data becomes

[1] τ_{Lag} represent lag time in this thesis and τ is used in paper 2 and 4.

$$G(\tau_{Lag}) = \sum \delta N(t)\delta N(t+\tau_{Lag}) \quad (13)$$

where

$$\delta N(t) = N(t) - \langle N(t)\rangle. \quad (14)$$

According to Elson and Magde, "The rates at which $\phi(\tau)$decays to zero with increasing τ give a measure of how quickly diffusion and chemical reaction change the configuration of the system. Assuming a three-dimensional Gaussian distribution for the excitation volume generated by the two-photon process, the fluorescence correlation function $G(\tau_{Lag})$ is defined as

$$G(\tau_{Lag}) = \frac{G(0)}{1+\frac{\tau_{Lag}}{\tau_D}} \quad (15)$$

where τ_D is characteristic diffusion time of the fluorophore. This means that the shape of the FCS curve which is how fast the autocorrelation function is decaying provides the information about characteristic diffusion time τ_D. The average number of molecules detected in the excitation volume, *N* is inversely proportional to the amplitude of the autocorrelation function *G(0).*

In paper 1, a practical guideline to implement MPM-FCS is explained by highlighting the theoretical and practical perspectives. Paper 2 demonstrates how MPM-FCS can be implemented to study viscosity dependent diffusion characteristics. In addition, this technique is validated in collagen matrix by measuring the viscosity, ultimately targeting the complex biological samples.

Chapter 4. Biomedical Applications

4. Biomedical Applications

4.1. *In vitro* studies and cellular autofluorescence

Human skin which is the largest organ in the body and has been a topic of research for many years and it facilitated to study of topical drug delivery, tissue engineering, skin cancer and many other applications [60-63]. Today in the field of tissue engineering, the novelty is the development of an organ-on-chip model where three-dimensional cell cultures imitate the microenvironment of particular health conditions are implemented [64, 65]. These models are beneficial for targeted drug delivery studies and ultimately developing organ models. *In vitro* skin culture models are such kinds of systems where the three-dimensional cellular models are grown in a sterile environment [63, 66].

There is a need to develop non-invasive microscopic techniques to examine these models to understand the morphological features as well as fundamental details of the cell. The traditional histopathological analysis is not sufficient due to its inherently invasive nature. As discussed in chapter 3, MPM-FLIM is a good non-invasive label-free technique for studying *in vitro* skin models. MPM-FLIM utilizes the autofluorescence originating from intrinsic fluorophores such as nicotinamide adenine dinucleotide (NADH), flavin adenine dinucleotide (FAD), and keratin [67-69]. NADH and FAD are prominent cellular metabolic markers. According to the previous reports, the fluorescence lifetime changes depend on whether they are in free (unbound) form or bound to enzyme or protein as shown in the below table,

Table 4.1: *Details of the common intrinsic cellular fluorophores*

Cellular fluorophore	**Peak excitation wavelength (nm)**	**Peak emission wavelength (nm)**	**Fluorescence lifetime (ns)**
NADH	340	470	0.2-0.6 (free) [44, 70, 71] 1-4.5 (bound) [44, 70, 71]
FAD	405	530	2.3-3.6 (free) [44, 71] 0.3-0.5 (bound) [44, 71]
Keratin	480	525	1.4 [72]

As seen in the table there is high variability in the fluorescence lifetime of NADH itself which makes it difficult to interpret the FLIM data. Moreover, the two-photon characteristics of keratin are scarce which is a topic of interest in paper 4. Proper characterization of these cellular fluorophores is important to understand how to differentiate them in the light of spectral and fluorescence lifetime overlap. Therefore, two-photon spectral and fluorescence lifetime characterizations of cellular monolayers of keratinocytes and fibroblasts are performed using

MPM-FLIM. Keratinocytes are one of the main cell types constituting the epidermis of the skin. The results from this study are demonstrated in chapter 6.

4.2. Malignant melanoma and sentinel lymph nodes

Malignant melanoma is the most aggressive form of skin cancer and is caused by the malignancy of melanin-producing melanocytes in the skin [73]. According to the studies, the incidence of melanoma across the globe is increasing year by year and Sweden is in the top five listed countries [74, 75]. Malignant melanoma initially starts as a small lesion (the primary tumor) in the skin and can develop in lymph nodes by metastasizing through the lymphatic system in the later stages. The survival rate is high if the metastasis is diagnosed in the early stage and the success of the treatment depends on diagnosing the stage of metastasis [75-78].

The standard treatment procedure for malignant melanoma is examining the primary tumor followed by the sentinel lymph node biopsy for staging the metastasis [78-80]. And sentinel lymph node is the first metastasized lymph node. But this invasive procedure of sentinel lymph node biopsy has many limitations. The histopathological analysis is time-consuming and highly intensive work. Moreover, in some cases, the unwanted removal of lymph nodes may happen which leads to several side effects such as infection, lymphedema, and prolonged wound healing [81, 82]. Therefore, it is very crucial to develop non-invasive optical techniques to diagnose malignant melanoma at an early stage to improve the treatment. Hence, MPM-FLIM has been applied to investigate the metastasis in sentinel lymph nodes extracted from malignant melanoma patients. The results from this study are discussed in chapter 6.

Chapter 5. Methods and Materials

5. Methods and Materials

Two different MPM set-ups have been utilized in this thesis as described in the following section.

5.1. Commercial MPM set-up

In paper 4, a commercial MPM setup (LSM 710 NLO, Carl Zeiss, Jena, Germany) system equipped with a fs-pulsed laser (InSight Deepsee, Spectra physics) tunable in the range 680-1300 nm was used for facilitating spectral excitation scan. For this purpose, a spectral detector (QUASAR, 34 channels, 9 nm resolution) in the range of 421–693 nm was employed. This special feature helped to obtain the emission spectra from the samples and to separate the fluorescence signals from different fluorophores.

5.2. Experimental MPM set-up

An MPM-experimental set-up is used in paper 1-4. The schematic diagram of the main experimental MPM set-up for implementing FLIM and FCS in this thesis is shown in **figure 6** and the list of components is given in **table 5.1**. As discussed in chapter 3, the main part of the MPM setup is a fs pulsed near infra-red laser and Ti: Sapphire laser (Tsunami, Spectra-Physics, ~80 fs, 700-900 nm) pumped by solid-state Nd:YAG laser (Millenia x laser, spectra physics,532 nm) is the source of two-photon excitation in this work. The set-up is equipped with two GaAsP detectors (Hamamatsu) which are interfaced to time-correlated single-photon counting modules SPC 150 (TCSPC, Becker&Hickl, Berlin, Germany), enabling FLIM and FCS.

5.Methods and Materials

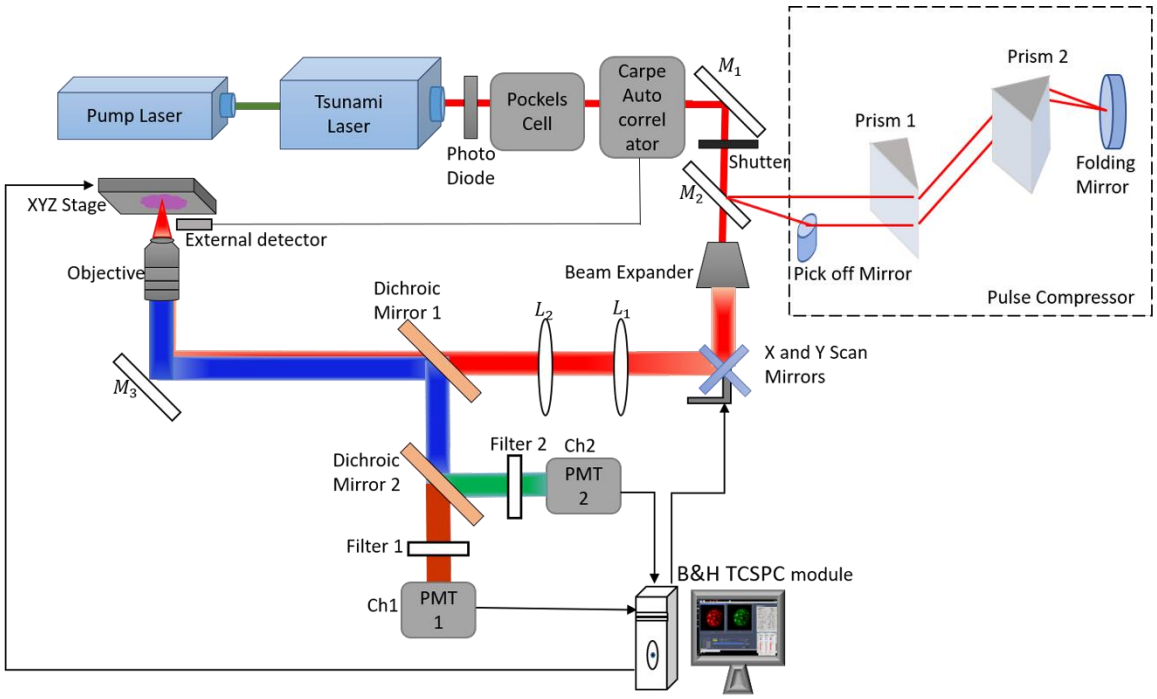

Figure 6. *Schematic diagram of the experimental multiphoton microscopy setup (image reprinted with permission from [83].*

Table 5.1*. Parts of the experimental multiphoton microscopy setup*

Name of the component	**Model, Manufacturer**	**Specification**
Solid-state Nd:YAG laser	Millenia, Spectra Physics	>10 W,532 nm
Ti:Sapphire laser	Tsunami, Spectra Physics	80 MHz, 700-1000 nm
Photodiode	APS-100-01, Becker&Hickl	
Pockels cell	350-80LA, Conoptics	
Spectrometer	Avaspec 3648, Avantes	200-1100 nm
Beam expander	BE05M-B, Thorlabs	5x Magnification
Scanning mirrors	GVS002, Thorlabs	5 mm Diameter
Microscope Objective	C "Achroplan" NIR, Carl Zeiss Olympus	40x/0.8 W D=0,17 10x/0.30 63X 20X
Dichroic mirror	Semrock, Bright line	509 nm and 550 nm
Filters	Semrock, Bright line	447/60 nm 525/50 nm 580/150 nm
Photo-multiplier Tubes	2x H7422P-40 MOD, Hamamatsu	300 - 720 nm
Data collection Cards	SPC-150, Becker&Hickl	10 MHz
Software	SPCM, Becker&Hickl	V.9.67
Autocorrelator	Carpe, APE, Berlin	700-1200 nm
Femto control kit	APE, Berlin	30 fs-3.5 ps

5.Methods and Materials

A major adaptation of the MPM set-up was pulse width measurement and dispersion compensation, done by installing a carpe autocorrelator and a femtocontrol unit (APE, Berlin, Germany). The carpe autocorrelator was chosen based on the ability to measure pulse width at laser output as well as at the sample location. The femtocontrol unit contains a prism pair, able to compensate the pulse dispersion in the optical path between laser and the microscopic stage for the sample holder as described in **table 5.2**. Compensation for pulse dispersion leads to higher two-photon absorption probability and thereby improved signal-to-noise imaging.

Table 5.2. *Pulse width measurements at different locations in MPM set-up obtained from Gaussian fitting.*

Location of measurement	**Pulse width (fs)**		
	at 750 nm	**at 800 nm**	**at 850 nm**
Laser output	79±2	75±1	80±2
Sample stage (uncompensated)	350±5	360±5	380±5
Sample stage (compensated)	110±2	100±2	105±2

Figure 7 shows the effect of pulse compression on the FLIM image of the root of a convallaria sample. As can be seen from figure 7.a, the image after pulse compression is clearer and crisper compared to the image taken before compressing the pulse. This confirms that the lifetime value is not affected but the signal strength strongly depends on the pulse width of the laser.

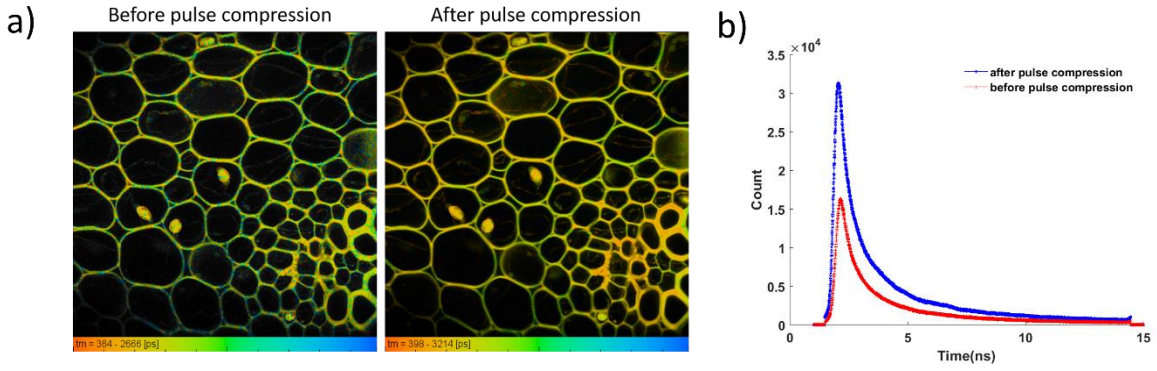

Figure 7. *Effect of pulse compression on a) FLIM imaging and b) photon count of convallaria sample before (~360 fs) and after (~100 fs) pulse compression at 800 nm and 250 mW power, 512x512 pixels, Field of view ~150x150 µm, and b) effect of pulse compression on photon count during imaging convallaria.*

5.3. Implementation of FLIM and FCS in TCSPC method

In this thesis, the time-correlated single-photon counting (TCSPC) [47] detection method is utilized for implementing FLIM and FCS in an experimental MPM setup. For this purpose, highly sensitive GaAsP detectors (H7422P-40 MOD, Hamamatsu) are used to detect single photons from the fluorescence emission even though the dynamic range of these detectors is limited as compared to the ones in the commercial MPM systems. The detectors are calibrated for optimum gain in the current MPM set-up. Two TCSPC computer cards (SPC 150, Becker&Hickl, Berlin, Germany) are installed and interfaced to the detectors and scanning mirrors. A detailed description of the hardware and software developed for TCSPC is available in the handbook from Becker and Hickl [48]. The basic working principle of the TCSPC system is shown in **figure 8.** As shown in the figure, the time of arrival of the photons with respect to the laser pulses and the position of the scanned laser pulses at the time of photon detection is registered. After many photons are collected and registered in the memory of the TCSPC module, a photon distribution is created. FLIM images are obtained from the photon distribution at each pixel and FCS curves are obtained by correlating the photon arrival time.

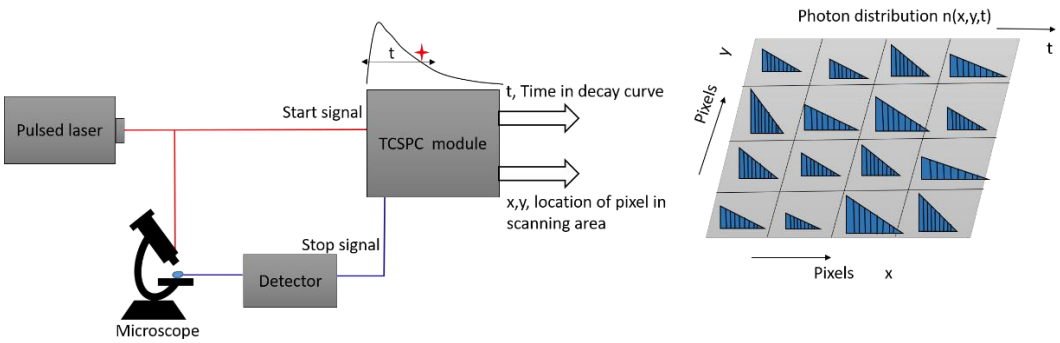

Figure 8. *Basic working principle of TCSPC detection method. Figure inspired from [47].*

5.4. Fluorescence lifetime imaging (FLIM)

5.4.1. Materials for FLIM studies

In paper 3, human lymph node samples were obtained from a biobank at the Department of Pathology, at the Sahlgrenska University Hospital in Gothenburg, Sweden. Both metastasis positive and negative lymph nodes were included as a part of an ongoing study approved by the local ethics committee (University of Gothenburg, No 145-16). An example of human

lymph node sample used in the study is shown in **Figure 9**. A detailed description of samples and patient demography are provided in paper 3.

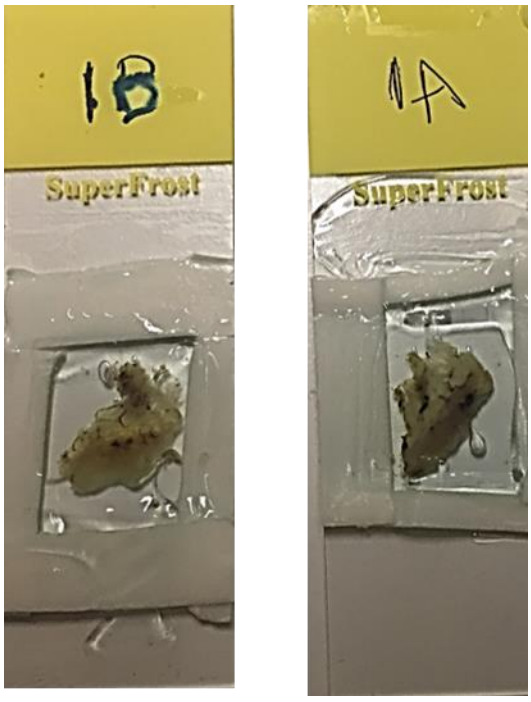

Figure 9. *Sentinel lymph nodes are mounted on a microscopic slide with ultrasound gel. Image Credits – Despoina Kantere.*

In paper 4, commercially available neonatal human epidermal keratinocytes (HEKn, Thermo Fisher Scientific) and adult human dermal fibroblasts (HDFa, Thermo Fisher Scientific) were used for the MPM-FLIM experiments. The cells were grown on glass-bottom dishes by fellow Ph.D. student Monika Malak in a sterile cell culture lab at the University of Gothenburg, Sweden. The detailed protocol for all cell culture experiments is provided in paper 4. My role was to perform the FLIM imaging using an experimental MPM setup. During the imaging, the cell dishes were placed in a humidified incubator installed on the microscope at 37°C.

5.4.2. FLIM data analysis

The data files were collected as .sdt files obtained from SPCM64 (Becker & Hickl) software and FLIM images were analyzed by SPCImage software (v 9.82, Becker & Hickl). A screenshot of the SPCImage software is given in **figure 10**. As seen in the figure, the MPM intensity and FLIM image of a Convallaria root sample is demonstrated with the distribution of fluorescence lifetime over the entire image. As seen in the FLIM figure, the color in the FLIM image represents the fluorescence decay time and brightness corresponds to the photon count. Also, lifetime information from each pixel can be extracted. A single exponential or

double exponential decay model can be selected based on the samples. A FLIM image of a Convallaria root sample taken using MPM equipped with a TCSPC card is shown in **figure 10.** As seen in the figure, the color in the FLIM image represents the fluorescence lifetime at each pixel. The fitting of the fluorescence decay was optimized by testing on several pixel positions by keeping the reduced chi square (χ^2) value as close to 1 by optimizing the fitting paraments (shift, offset and scatter). The value of χ^2 is a measure of the extent of correlation between the observed value and estimated value with the least error variance. Hence, there is a range of lifetime values and pre-exponential factors that could potentially fit the decay curve. Therefore, careful measures need to be done during FLIM analysis and reflect on this fact when interpreting the FLIM data. One possible way is to keep an eye on a good fitting curve (Fig 10.d) and the variance (Fig 10.e). Raw data files containing all the information such as pre-exponential factors, lifetime values, lifetime distribution, fitting paraments, intensity image, and FLIM images can be extracted from SPCImage software and are re-processed in MatLab (vR2020b, MathWorks Inc.).

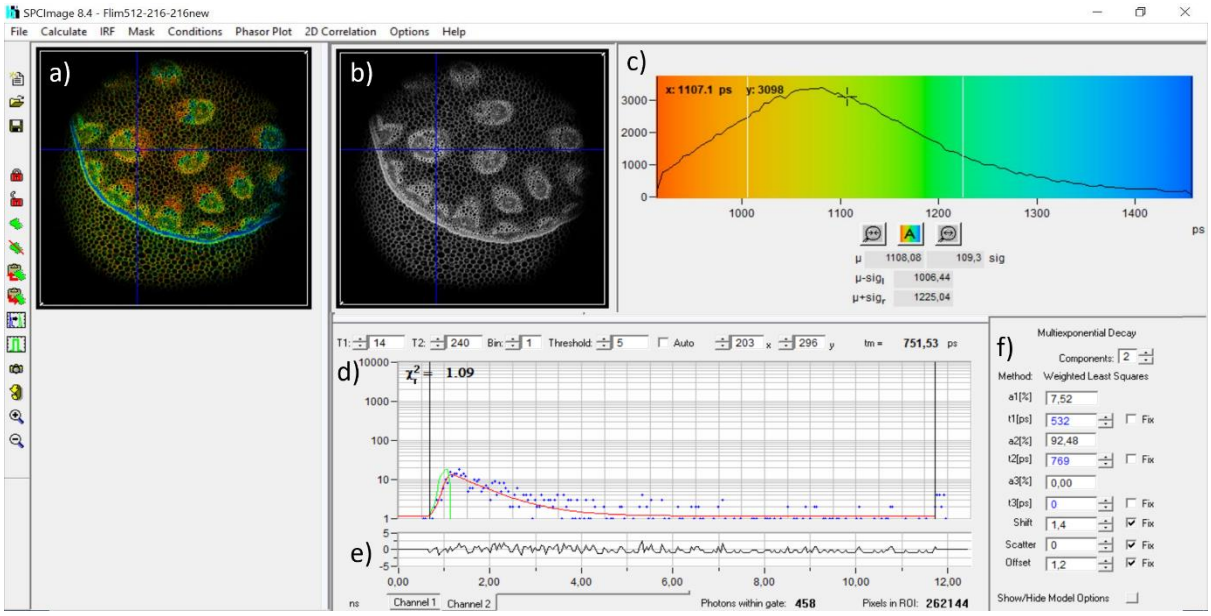

Figure 10. *FLIM analysis using SPCImage software. MPM-FLIM image (a), intensity image (b) of Convallaria root sample along with fluorescence lifetime distribution (c), decay curve (d), error variance (e), and fitting model parameters.*

In paper 3, the potential of the MPM-FLIM technique to diagnose melanoma metastasis in human sentinel lymph node tissue from melanoma patients is validated. Paper 4 explores the characterization of keratinocytes and fibroblasts at different excitation wavelengths (725 nm to

810 nm) to define the contribution of keratin in 2PE imaging of keratinocytes using MPM-FLIM.

5.5. Fluorescence correlation spectroscopy (FCS)

In papers 1 and 2, Rhodamine B was used as a potential fluorophore for all the FCS measurements. **Figure 11** shows a screenshot from SPCM64 software demonstrating FCS traces during the experiments. As seen in the figure, both fluorescence decay trace, as well as the FCS curve, is visible simultaneously which confirms the reliability of the measurements. In addition to that, the photon count (Fig 11.c) indicates any other occurring effects such as photobleaching or saturation. A steady photon count around an average value is a measure of a good signal. The FCS curve (Fig 11.b) is generated by the multi-tau algorithm which is used for fast data acquisition. This is used as a quality control measure to verify the FCS curve during the experiments. Later .spc files from SPCM64 are processed in burst analyzer2 (Becker and Hickl) software for FCS data analysis where raw data files containing photon arrival time are extracted. A customized Matlab code based on a linear-tau algorithm for the analysis of FCS data obtained from the TCSPC module is developed as described in the appendix.

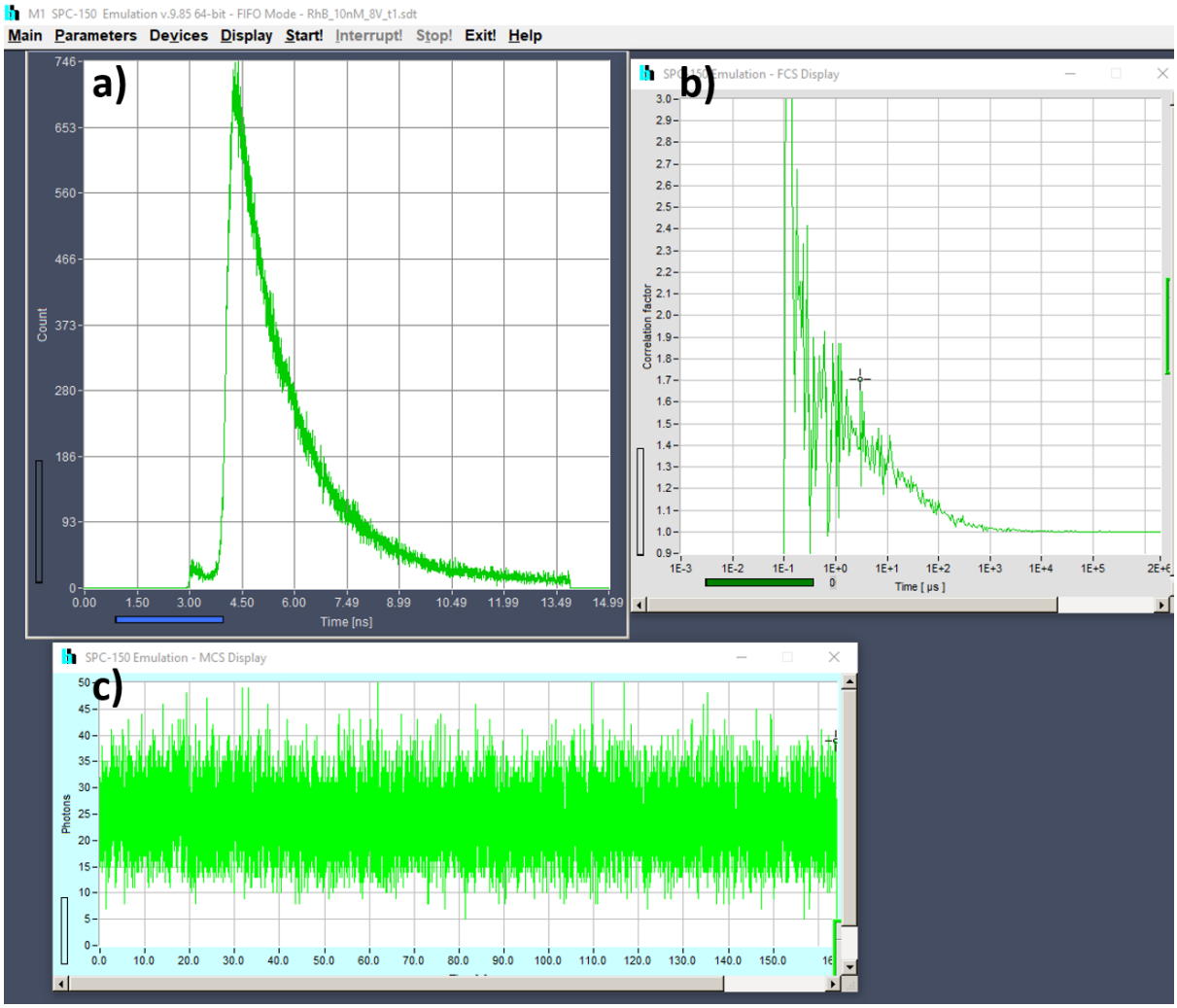

Figure 11. *Screenshot from SPCM 64 software during FCS measurements. Fluorescence decay (a), FCS curve (b), Photon count (c) as seen in a live FCS experiment.*

In the previous studies [30], FCS data fitting is done as follows,

$$G(\tau_{Lag})=1/[N(1+\frac{\tau_{Lag}}{\tau_D})(1+\tau_{Lag}/\omega^2\ \tau_D)^{0.5}] \quad 16$$

where $G(\tau_{Lag})$ is normalized autocorrelation function, N is the number of particles present in the focused volume, τ_D is translational diffusion time and ω is the ratio of the lateral and the axial radius of the excitation volume. In the case of 2PE, diffusion coefficient (D) can be determined [84] by the following equation,

$$D = \omega^2/8\,\tau_D. \quad 17$$

However, a simple data fitting model as used by Magde and Elson [23, 53] is used for all the FCS data fitting in this work. The data fitting model is as follows,

$$G(\tau_{Lag})_{simple} = \frac{G(0)}{1 + \frac{\tau_{Lag}}{\tau_D}} \quad 18$$

Stokes-Einstein equation [85] explains the diffusion in solution as follows,

$$D = \frac{k_B T}{6\pi\, \eta a} \quad 19$$

where, k_B is Boltzmann constant, T is the temperature in Kelvin, η is the viscosity of the solvent and a is the thermodynamic radius of the diffusing molecule. Thus, it is very clear that viscosity plays a major part in diffusion. Hence, considering the viscosity the translational diffusion time becomes,

$$\tau_D = \frac{\omega^2\, \eta}{8 D_w \eta_w} \quad 20$$

where, D_w is the diffusion constant measured in water at a viscosity of η_w.

In paper 2, this relationship between viscosity and diffusion time is validated by MPM-FCS measurements done in different water glycerol mixtures using Rhodamine B. In addition to that proof of principle to measure the viscosity from diffusion time is demonstrated by the FCS measurements performed in a collagen gel matrix.

Chapter 6. Results

6. Results

Four papers are included in this thesis. This chapter contains a summary of all the results and main findings are discussed. A detailed description is available in the appended papers.

6.1. MPM-FCS practical guideline (Paper 1)

In paper 1, different experimental conditions such as concentration range, numerical aperture of the objective lens, and laser excitation power are investigated. **Figure 12** shows the effect of numerical aperture on FCS measurements obtained from two different microscope objectives, 63X (NA1.2, working distance 0.28 mm) and 40X (NA 0.8, working distance 1.8 mm) by performing FCS measurements in Rhodamine B solution at different concentrations (10 nM, 20 nM, 40 nM). As seen in the figure, FCS data can be acquired using both the 63X and 40X objective lenses; however, the amplitude of the correlation function is higher for the 63X objective as compared to 40X. This is because a higher NA objective lens will generate a smaller excitation volume and contain fewer molecules giving rise to a higher *G(0)* value as explained in the theory section. Considering the impact of concentration, the FCS curve starts to deteriorate with the presence of oscillations (Fig 12.c) when the concentration is increased in the case of the 40X objective lens. Whereas the autocorrelation function and FCS curve remain stable as the concentration is increased to 40 nM (Fig 12.f) for 63X objective lens. Thus, this means that the adaptability of utilizing the long working distance 40X objective lens is lower as autocorrelation amplitude function and FCS curve is disintegrating if concentration increase further.

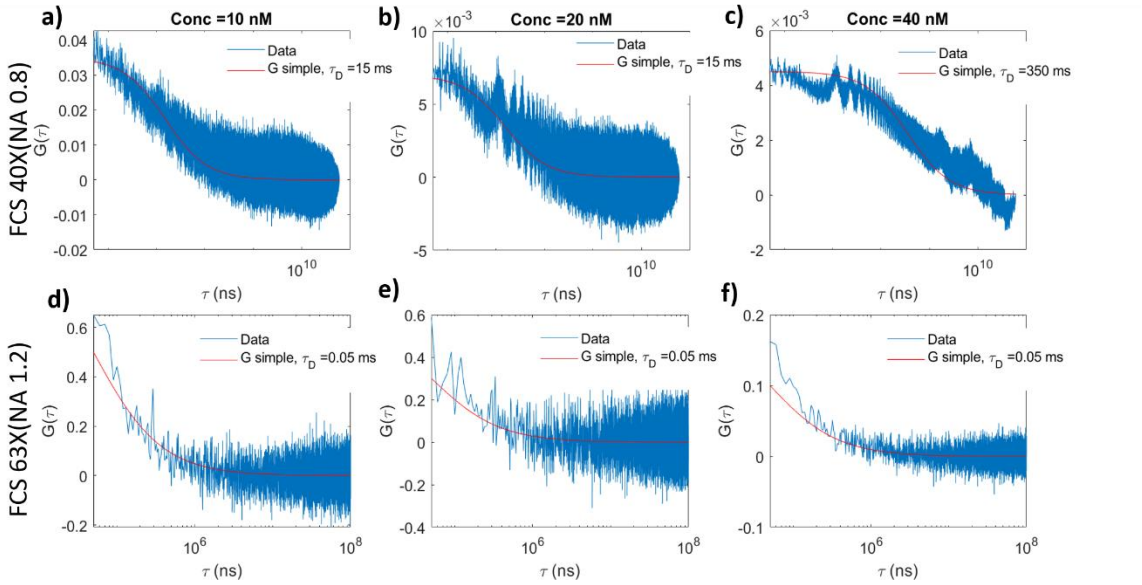

Figure 12. *The effect of concentration and numerical aperture of the objective lens on FCS data obtained from Rhodamine B solution at different concentrations (10nM, 20nM and 40nM) generated by different objective lenses 40X (NA 0.8) and (d-f) 63X (NA 1.2). Autocorrelation function data (blue) and fitted data (red) are shown. The data was obtained from the red channel (580/150 nm) at 800 nm excitation wavelength, 25mW excitation intensity.*

Considering these results, it is evident that objective lenses with lower NA are less suitable for FCS studies. However, it is possible to obtain FCS data at a lower concentration range, but rigorous calibration and prior knowledge is required.

Figure 13 demonstrates the effect of time binning on the autocorrelation function in the FCS curve and photon count per time bin obtained from TCSPC raw data from the measurements of Rhodamine B solution at 10 nM using the 63X objective lens. FCS data (Fig.13 f-j) and photon count per time bin (Fig 13.a-e) are plotted for different time binning varied from 10^3 – 10^6 ns as seen in the figure. It is clear from the figure that the autocorrelated data becomes noisy at a shorter time binning (Fig 13.f, 10^3 ns) which results in the loss of information. Thus, it certifies that proper selection of time binning is important to obtain relevant autocorrelation data and a better data fitting as suggested by Elson and Madge explained in the theory section [24].

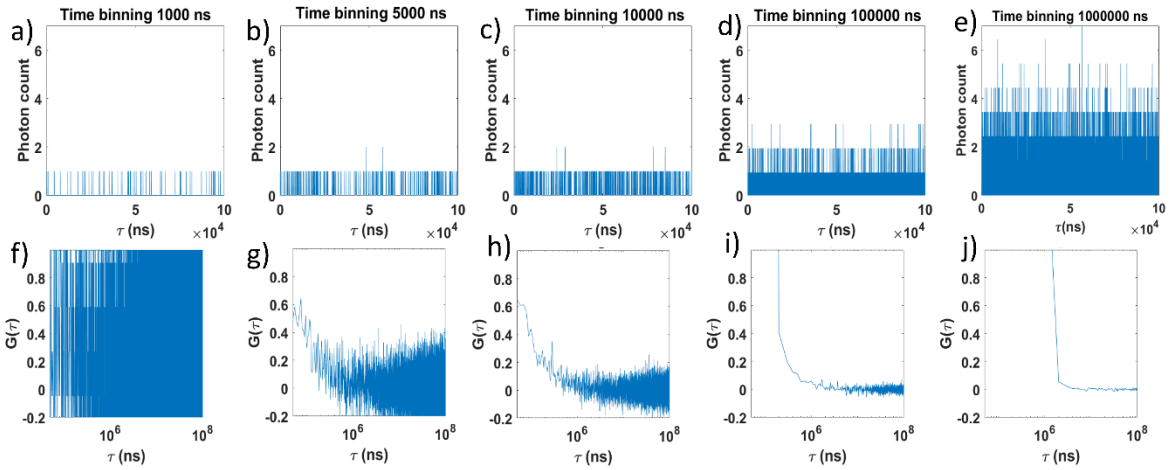

Figure 13. *The effect of time binning in the range 10^3 – 10^6 ns on photon count rate per time bin (a-e) and FCS data (f-j) acquired from Rhodamine B solution at concentration 10 nM. The data was obtained from the red channel (580/150 nm) at 800 nm excitation wavelength, 25 mW excitation intensity using a 63X (NA 1.2) objective lens.*

Similar to the previous explanation for the impact of time binning on FCS data, the photon count vector is sparse and binary at binning of 10^3 ns. This correlates with the loss of autocorrelation information for low binning (Fig 13.f). The photon counts per time bin start to increase above one when the binning is increased over 5×10^3 ns. Photon counts per time bin and noise level are improved when the binning is increased further. This confirms that data based on concentration fluctuations should follow Poisson statistics [86]. These results show that the optimum time binning for this experimental setup is around 10^4 – 10^5 ns.

Figure 14 shows the impact of excitation intensity on the FCS data and fitting parameters acquired by the 63X objective lens. As seen in the figure, the amplitude of autocorrelation function (*G(0)*) and average photon counts (*P*) are plotted as a function of normalized excitation power (I/I_0), where I_0 was defined as the lowest excitation power for each objective lens. As explained in the theory, the size of the excitation volume increases with an increase in excitation intensity [87]. Due to the inverse relationship between *G(0)* and *N*, the value of *G(0)* decreases as excitation power increases (Fig 14.a).

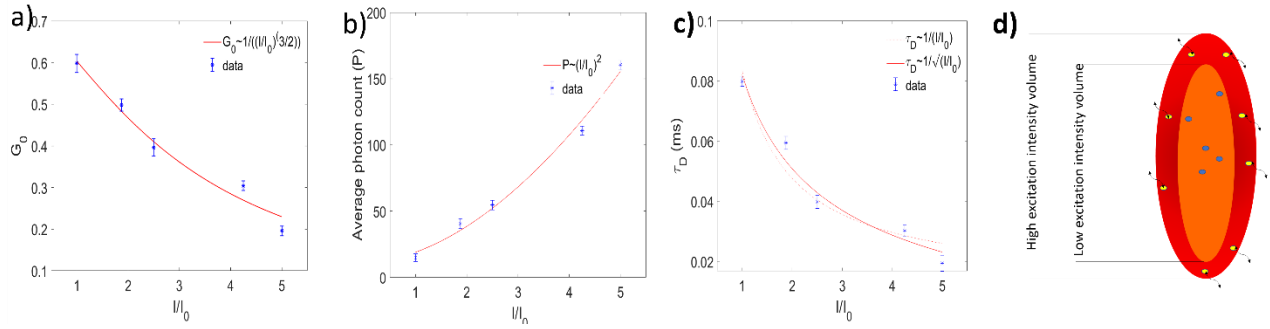

Figure 14. *Plot of the a) autocorrelation amplitude function G(0) acquired using simple data fit (G(0) ~$(I/I_0)^{3/2}$) and b) plot of average photon count c) plot of the diffusion time acquired using simple data fit (τ ~$1/(I/I_0)^{0.5}$ on autocorrelated data 10000 ns as a function of excitation power from experimental measurements of Rhodamine B solution (10nM), the 63X (NA 1.2) and d) illustration of the shape of excitation volume at different excitation power levels. Data points in blue and red lines are fitting.*

The impact of excitation intensity on diffusion time is investigated and the values of the diffusion time decrease when the excitation power is increased (Fig 14.c). The excited molecules diffuse through a longer distance at higher excitation intensity since the size of detection volume increase according to the previous theoretical investigations when considering saturation or photobleaching effects [87, 88]. However, as expected for two-photon excitation a quadratic behavior $(I/I_0)^2$ is observed when the effect of excitation intensity on an average photon count [16]. This means that there is no evidence of photobleaching or excitation saturation in our FCS data in contrast to other reports published earlier [87-89]. Thus, this surprising behavior of diffusion time possibly is due to an alternative interpretation of the FCS measurement, as shown by Fig 14.d. This hypothesis is based on the fact that slower diffusion time derives from fluorescence fluctuations of the molecules from the rim of the detection volume rather than the core. Whereas the molecules at the periphery of the observation volume travel a shorter distance and thus deliver faster correlation and diffusion time. The ratio of effective surface area to the size of the observation volume decreases at higher excitation levels (see supplementary data, paper 1). Diffusion time is proportional to the area when the diffusion constant remains the same as explained by the dimensional analysis of Fick's diffusion law [90]. This means that diffusion time is inversely proportional to the surface area to size ratio, i.e., the square root of the radius of the detection volume, and it is related to the normalized excitation power. This leads to a shorter diffusion time at higher excitation intensities. The discrepancy in diffusion times for 40X and 63X objective lenses most likely originate from these phenomena. Thus, a further theoretical examination is needed to compensate for this

effect to extend the applicability of MPM-FCS. Table 6.1 describes a summary of key results from this practical guideline for MPM-FCS measurements.

Table 6.1. *Summary of results main parameters and conditions for FCS measurements. Reprinted with permission from [67].*

Parameters	**Conditions**	**Observations and recommendations**
Objective lens	High NA objective lenses (NA>1) are preferred for FCS; however, for imaging MPM the long working distances normally restrict NA.	• Higher NA leads to fewer distortions in FCS data and more reliable diffusion measurements. • Lower NA (NA<1) objective lenses can be used but careful validation is required.
Concentration range	The concentration should preferably be in the nM range for FCS. But for imaging the concentration range can vary by several orders of magnitudes.	Concentration ranges need to be validated before measurements: • Autocorrelation trace should be devoid of oscillations or distortions that may appear at a higher concentration range. • The amplitude of the autocorrelation function *(G(0))* needs to be above the threshold value. • The measured translational diffusion time needs to be comparable with theoretical translational diffusion time.
Excitation power	In MPM-FCS the excitation power will determine the excitation and detection volume.	• Look for an inverse relationship of laser power on the measured diffusion time using a simple model fit. • Based on this relationship, find the threshold range of excitation power can be applied for certain objective lenses.
Time binning	TCSPC raw data has a sparse binary data format, and time binning is required to perform autocorrelation.	The optimal range of time binning should be validated for the specific experiments. • Photon count per time bin should increase above binary value • Photon distribution over time binning should follow Poison distribution.
Autocorrelation algorithm	Multi-tau and extended data fitting models have been proposed in the literature. Here it is shown that linear-tau and simple model fitting is preferred for the data analysis.	• Multi-tau view can be used for fast data assessment during acquisition • For data analysis, linear tau and simple model are preferable to enable systematic validation of the parameters above.

6.2. MPM-FCS for viscosity studies (Paper 2)

Paper 2 aims to demonstrate the effect of viscosity on diffusion time measurements of Rhodamine B in different water glycerol mixtures performed in MPM-FCS way. In addition to that, viscosity of collagen gel matrix is calculated from FCS data targeting complex biological systems. **Figure 15** shows a comparison of different FCS curves obtained for 10% (1.4 cP) and 50% (7.2 cP) glycerol samples along with diffusion time shown in the legend. As seen in the figure, 10% glycerol sample results in a faster diffusion time (0.07 ms) as compared to the second sample (50% glycerol) due to the viscosity difference. In addition to that, the amplitude of autocorrelation function *(G(0))* is in the same range for both FCS curves which points to the same amount of Rhodamine B molecules in the excitation volume. From these observations, it is evident that the MPM-FCS setup validates the approach to measure the diffusion time in different viscosity samples.

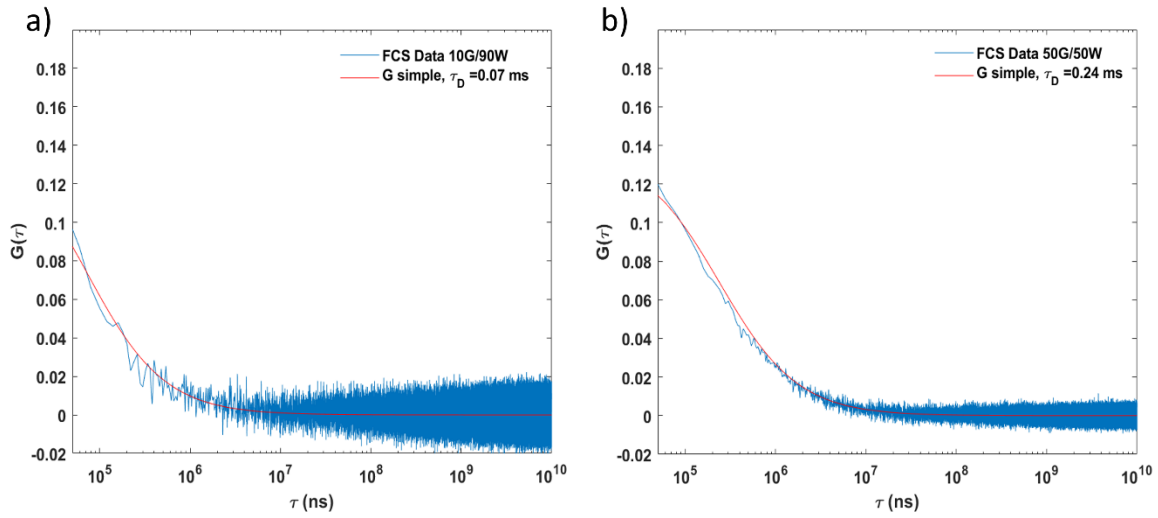

Figure 15. *Diffusion time (τ_D) extracted from FCS data of Rhodamine B (10 nM) in different ratios of water glycerol mixtures a) 10% and b) 50%. The diffusion time is extracted from FCS curve fitting parameters by equation 18 in section 5.5.*

Table 6.2 shows the viscosity (η_{exp}) calculated (section 5.5, equation 20) from diffusion time (τ_D) obtained from MPM-FCS measurements of Rhodamine B (10 nM) at different water glycerol ratios (0%-70%). As a control, the viscosity ($\eta_{control}$) of each water glycerol sample is measured using a rheometer at room temperature. As seen in the table, the viscosity (η_{exp}) values calculated from FCS data are in good agreement at lower glycerol percentage samples. Therefore, careful calibration is required for samples with higher viscosity values.

***Table 6.2**. Diffusion time (τ_D) and viscosity (η_{exp})extracted from FCS data of Rhodamine B (10 nM) for different water glycerol mixtures along with control viscosity values ($\eta_{control}$) measured from a rheometer.*

Glycerol: Water ratio (% v/v ratio)	**Viscosity$_{control}$ ($\eta_{control}$ cP)**	**Diffusion time (τ_D ms)**	**Calculated Viscosity$_{exp}$ (η_{exp} cP)**
0:100	1.0	0.05 ±0.002	1.0 ± 0.001
10:90	1.4 ± 0.01	0.07 ± 0.01	1.4 ± 0.011
30:70	2.8 ± 0.03	0.12 ± 0.005	2.4 ± 0.004
50:50	7.2 ± 0.95	0.24 ± 0.050	4.4 ± 0.048
70:30	20 ± 1.21	0.67 ± 0.030	13 ± 0.029

Figure 16 demonstrates the relationship between viscosity and diffusion time. The diffusion time obtained for Rhodamine B at 10 nM concentration in different water glycerol mixture solutions using MPM-FCS and corresponding control viscosity ($\eta_{control}$) are plotted in the figure. This plot is fitted to a straight line with a slope of 0.032 ms/cP points to a linear relationship as described by the Stokes Einstein equation (equation 19, see section 5.5). The important finding to be considered is that the radius of the diffusing molecule can be extracted from Stokes Einstein equation by inserting the diffusion coefficient (*D*, $4x10^{-10}$ m^2/s [91]) of Rhodamine B, and slope of the plot (see the supplementary data, paper 2). And the radius of the Rhodamine B molecule is calculated as 1 nm which is in agreement with the literature value (~1 nm) [92].

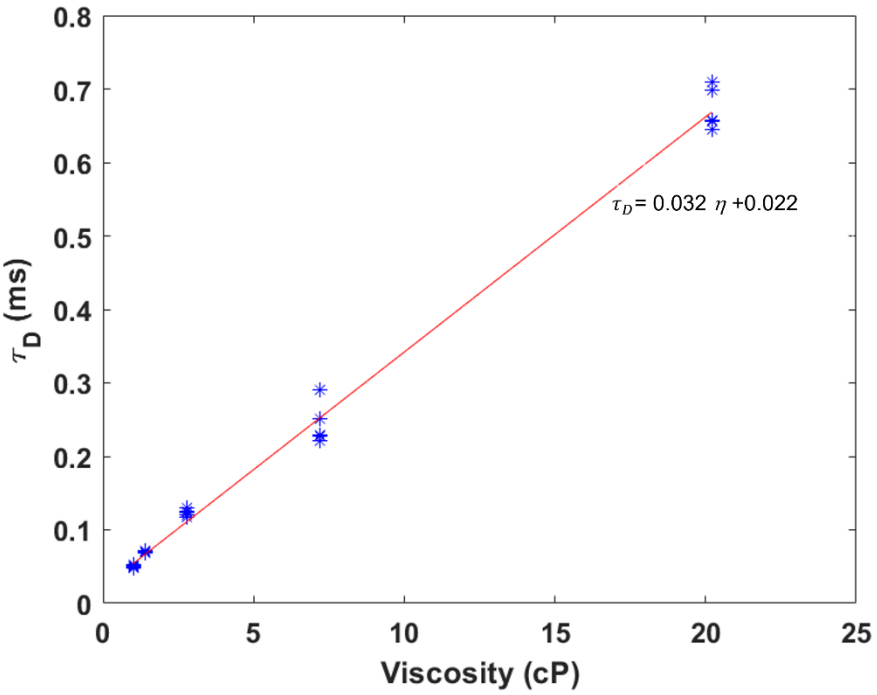

Figure 16. *Effect of viscosity on diffusion time obtained from MPM-FCS measurements performed for Rhodamine B (10 nM) in different water glycerol mixtures. The data points (blue, from 5 different measurements) are fitted to a straight line (red) with a slope of 0.032 ms/cP.*

Two collagen samples (1 mg/ml and 4 mg/ml) were used to demonstrate the proof of principle to measure the viscosity from diffusion time in the MPM-FCS method. The diffusion time of Rhodamine B (10 nM) in collagen samples were extracted from the FCS curves and is visualized in **figure 17**. As seen in the figure, sample 1 (collagen 1 mg/ml) result in a faster diffusion time (0.085 ms) as compared to sample 2 (collagen 4 mg/ml) due to the difference in viscosity. The viscosity of these collagen samples were obtained from the calibration graph (figure 16). And the viscosity was calculated as 2.0 ± 0.04 cP for the sample whereas for sample 2 is 8.1± 0.12 cP.

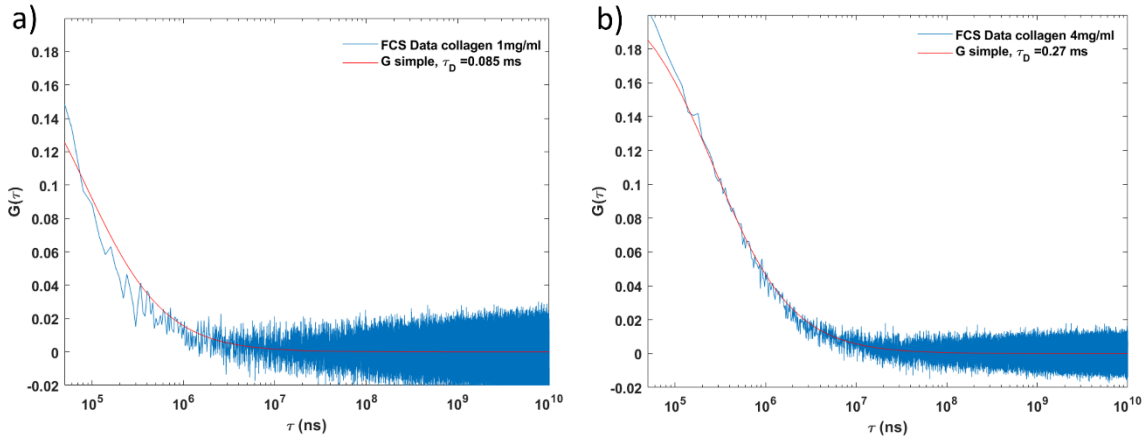

Figure 17. *FCS curve obtained for two different collagen sample a) 1 mg/ml b) 4 mg/ml. The FCS data was obtained from the red channel (580/150 nm) at 800 nm excitation wavelength, 25 mW excitation intensity.*

The results from paper 2 show the potential of MPM-FCS method to measure the viscosity of sample under examination from diffusion time measurements. The next stage is extending this approach in complex biological samples, and it is discussed in chapter 8.

6.3. MPM-FLIM for malignant melanoma (Paper 3)

The potential of MPM-FLIM to diagnose melanoma metastasis was investigated in paper 3. The study was performed using MPM-FLIM *ex vivo* investigating five sentinel lymph node tissue samples, three malignant melanoma positive and two negative sentinel lymph nodes derived from melanoma patients. FLIM images revealed fluorescence lifetime from inherent fluorophores in the sentinel lymph node tissue and correlated with histopathological morphological features from metastasized and non-metastasized sentinel lymph node tissues.

Figure 18 demonstrates comparison of MPM intensity and FLIM images obtained from one of the metastasized (Fig 18.b-d) and non-metastasized sentinel lymph node (Fig 18.g-i) tissues together with hematoxylin and eosin-stained (H&E) slide image (Fig 18.a and Fig 18.f). Corresponding fluorescence lifetime distributions from the MPM-FLIM images of the same positive (Fig 18.e) and negative (Fig 18.i) sentinel lymph node tissues are included in the figure. As observed in the figure, MPM intensity image (Fig 18.b) and FLIM image (Fig 18.c and Fig 18.d) from metastasized sentinel lymph node tissue obtained from channel 1 (580/150 nm) and channel 2 (525/50 nm) are presented respectively. Atypical cells with varying sizes (highlighted in Fig 18.c) which is known as pleomorphism are visible in the metastasized sentinel lymph node tissue as similar to hematoxylin and eosin-stained (H&E) slide image (Fig 18.a). A possible

mitosis as highlighted (*) seen in the Fig 18.c supports the presence of metastasis in this sentinel lymph node tissue. As a control sample, MPM-FLIM images from one of the melanoma negative sentinel lymph node tissues are presented from channel 1 (Fig 18.h) and channel 2 (Fig 18.i) together with MPM intensity image (Fig 18.f). The negative control sample exhibit a more homogenous tissue matrix as compared to the metastasized sentinel lymph node tissue. This homogenous negative tissue shows hardly discernable small cells (~7 µm) most likely representing lymphocytes, similar to the corresponding H&E-stained section (Fig 18.f).

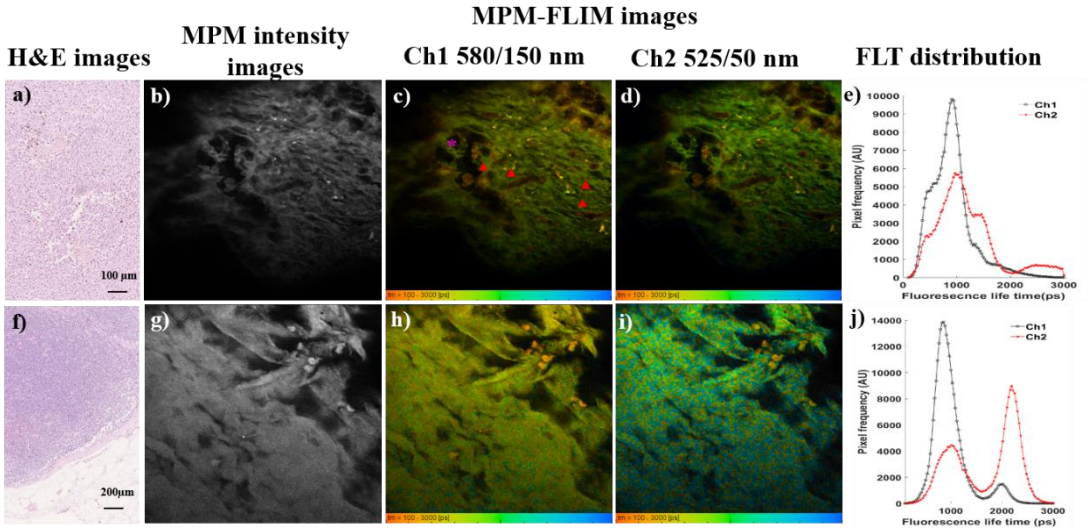

Figure 18. *Comparison of MPM-FLIM data extracted from metastasized (b-e) and non-metastasized (g-j) sentinel lymph node tissue together with H&E-stained histologic section (a and f). MPM intensity, FLIM images and corresponding fluorescence lifetime distributions are obtained from channel 1, 580/150 nm (b-c and g-h), channel 2, 525/50 nm (d and i). Atypical cells (Δ) and possible undergoing mitosis (*) in positive sentinel lymph node tissue are highlighted in (c). MPM and FLIM data acquired using 780 nm excitation. Field of view: (b, c, d) ~ 250x250 µm, and (e) 70 x 70 µm. False color scale lifetime data, 256-time channels, ranging from 100 - 3000 ps. Images reprinted with permission from [93].*

The acquired fluorescent lifetime distributions (Fig 18.e&j) obtained from both positive and negative sentinel lymph nodes tissues from two spectral channels most likely correspond to signals from NADH and FAD. In contrary to positive sentinel lymph node, a bimodal fluorescence lifetime distribution (Fig 18.j) is observed in the negative sentinel lymph node tissue. As discussed in previous chapter 4, the observed bimodal fluorescence lifetime distribution most likely corresponds to NADH and FAD in the two different spectral channels; the short lifetime (300 – 2000 ps) corresponds to NADH free and the long lifetime is probably from FAD (> 2000 ps) [40, 43, 94].

Figure 19 represents MPM intensity and FLIM images obtained from another positive sentinel lymph node tissue. As highlighted (Δ) in Fig 19.b, atypical cells showing pleomorphism are seen which certify the metastasis in this tissue and it is difficult to conclude only from the MPM intensity image. A sequence of bright cells without discernable nuclei exhibiting short fluorescence lifetime value (~ 600 ps) is clearly visible in orange-yellow color as highlighted (→) in Fig 19.b are possibly erythrocytes in the blood vessel. This shows the potential of MPM-FLIM to identify atypical cells and other structures based on morphological features together with lifetime information from each pixel.

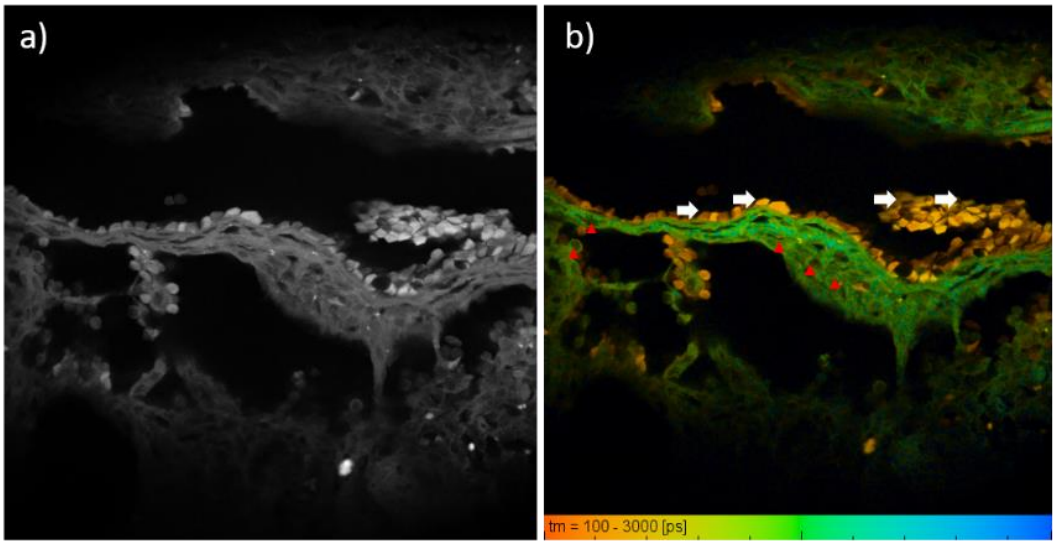

Figure 19. *MPM intensity (a), FLIM image (b) obtained from channel 1, 580/150 nm extracted from a metastasized sentinel lymph node tissue showing the atypical cells (Δ, red color) and blood vessel (→, white color). Field of view: 350x350 µm. False color scale fluorescence life-time data, 256-time channels, ranging from 100 - 3000 ps. MPM and FLIM data acquired at 780 nm.*

The results from this exploratory study demonstrates that MPM-FLIM based on autofluorescence has the potential to visualize melanoma metastasis in human sentinel lymph node tissue. The lifetime information seems to be a critical parameter when distinguishing between different cell types in the sentinel lymph node tissues. Morphological features together with fluorescence lifetime enabled to differentiate malignant atypical cells, healthy lymphocytes, blood vessels and erythrocytes in the lymph node. It should be noted that the lifetime values reported deviate slightly from the literature values. One plausible explanation is sample treatment during fixing and deparaffinization. Therefore, further experiments (see Chapter 8) on fresh lymph node tissues are required to validate the approach as a diagnostic tool for early staging of malignant melanoma together with histopathological analysis.

6.4. MPM-FLIM for keratinocytes (Paper 4)

In paper 4, MPM-FLIM characterization of intrinsic cellular fluorophores such as NADH, FAD and Keratin was performed. Spectral and fluorescence lifetime details of these intrinsic cellular fluorophores are described in chapter 4. MPM-FLIM characterization is beneficial to reduce the spectral cross talk between the excitation and emission spectra of the intrinsic fluorophores. For this purpose, the intrinsic cellular fluorophores in solution form are excited at different wavelength (725 nm, 750 nm, 780 nm, 800 nm and 810 nm) detected in two channels (Blue channel 445/65 nm and red channel 580/150 nm). **Figure 20** shows the average fluorescence lifetime values of free NADH, free FAD, NADH and FAD mixture, and keratin in solution obtained from MPM-FLIM data. Single exponential decay was applied for fluorophores (free NADH, free FAD and keratin) in solution and biexponential decay was applied for mixture of fluorophores (NADH and FAD, NADH and Keratin). The data for the mixtures are presented as amplitude averaged fluorescence lifetime (see equation 6, theory section). The fluorescence lifetime distribution histograms from both channels for all excitation wavelengths are presented in paper 4 (see supplementary materials).

6.Results

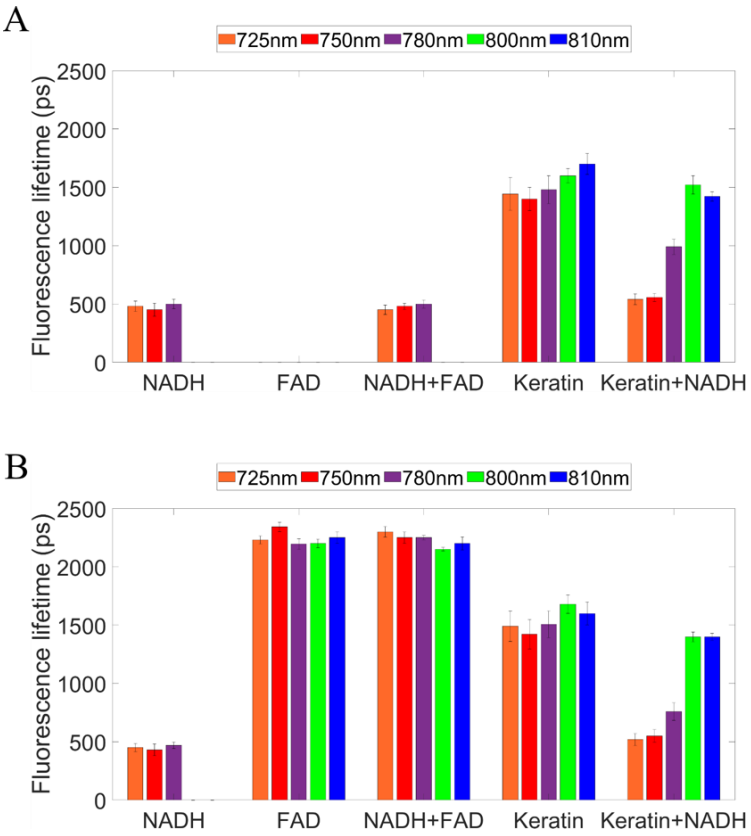

Figure 20. *Average fluorescence lifetime obtained from different intrinsic cellular fluorophores in solution (NADH, FAD, NADH and FAD mixture, and keratin) extracted from different channels (A) blue channel (445/60 nm), and (B) red channel (580/150 nm) at various excitation wavelengths (725 nm,750 nm,780 nm, 800 nm, and 810 nm).*

As expected NADH was detected in both the channels and free NADH in solution resulted in a short lifetime component around 0.5 ns for all the excitation wavelengths. In the case of FAD, a fluorescence lifetime around 2 ns was detected in the red channel alone. Whereas for NADH and FAD mixture, a short lifetime component of 0.5 ns (NADH) in the blue channel, and a long lifetime component around 2 ns (FAD) in the red channel. Interestingly Keratin in solution was excitable at all wavelengths and a fluorescence lifetime around 1.5 ns was shown. Now the challenge is to separate the fluorescence lifetime signal between NADH bound (1-2 ns) and Keratin. As a first step, NADH and Keratin mixture were investigated. The results have shown a shorter lifetime of 0.5 ns (NADH free) at 725-750 nm and 1.0 ns (at 780 nm) 1.5 ns (800 nm and 810 nm). This points towards the complexity of FLIM data interpretation in cellular samples.

To understand the characteristics of intrinsic cellular fluorophores in keratinocytes (HEKn) monolayer MPM-FLIM was performed at different wavelengths as like fluorophores in

solution. **Figure 21** shows the intensity and MPM-FLIM images of keratinocytes (HEKn) obtained from both channels (blue 445/60 nm and red 580/150 nm) together with fluorescence lifetime distribution histograms. As seen in the figure, fluorescence lifetime distribution is excitation dependent. The fluorescence lifetime is shifted from around 1 ns to 1.5 ns which is dominantly visible at the excitation wavelengths 800 nm and 810 nm in both the channels.

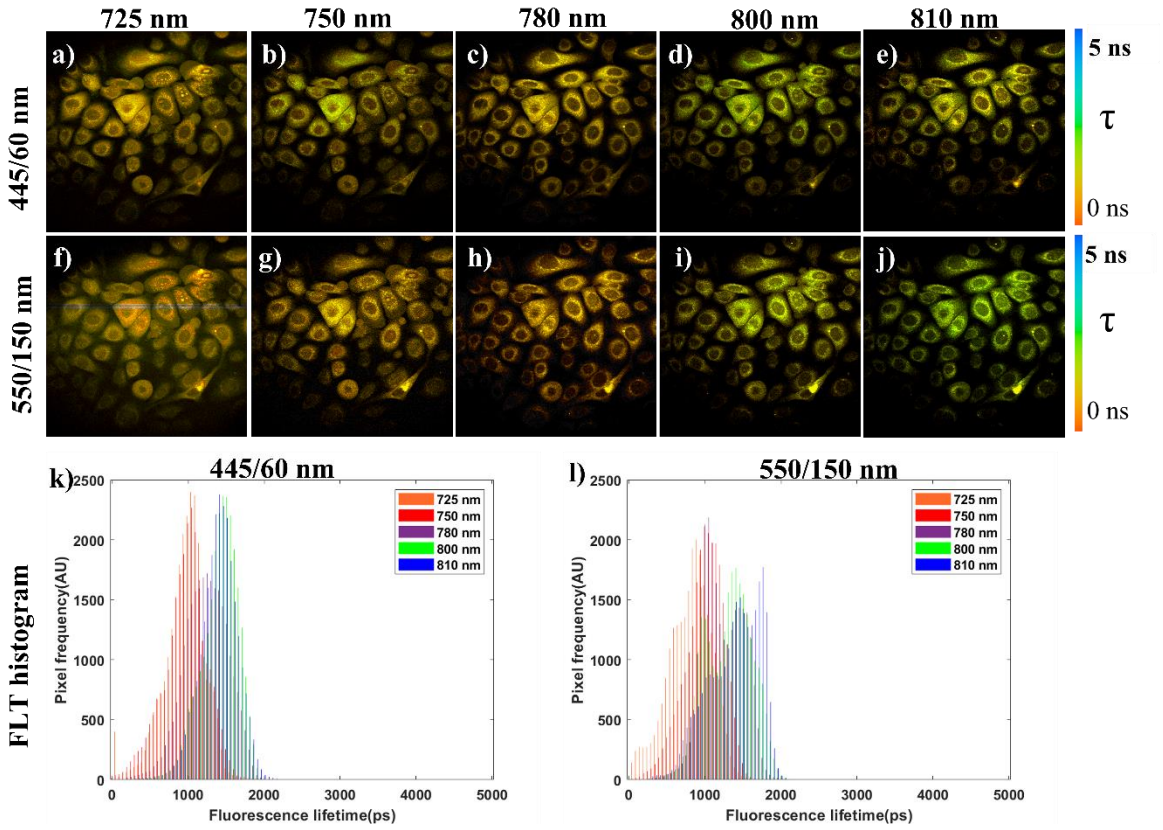

***Figure 21**. MPM -FLIM images of keratinocytes at different excitation wavelength (725 nm, 750 nm, 780 nm, 800 nm and 810 nm) obtained from blue (445/60 nm) and red (580/150 nm) channel along with corresponding fluorescence lifetime histograms. Brightness and contrast in the images were adjusted for clarity. Field of view is around 350 x 350 µm. False-color scale fluorescence lifetime ranging from, 256-time channels. The fluorescence lifetime distribution histograms show the average fluorescence lifetime distribution acquired from images of three biological replicates.*

This observed shift in fluorescence lifetime in MPM-FLIM data is comparable with the shift observed in NADH and keratin mixture (Fig 20). It is challenging to interpret this observation as the fluorescence lifetime of bound form of NADH is 1-4.5 ns [44, 70, 71]. Therefore, similar excitation-dependent MPM-FLIM imaging was performed in fibroblasts monolayers (see paper 4). But the shift in fluorescence lifetime was between 0.5 ns and 1 ns and 1.5 ns not present. Thus, the fluorescence lifetime around 1.5 ns at 800 nm and 810 nm may be coming

from keratin as it is an important cytoskeletal component in keratinocytes which is not in the fibroblasts.

An siRNA silencing of both KRT5 and KRT14 genes which should lead to the decrease of keratin levels in keratinocytes was performed. This procedure was done to verify origin of the fluorescence lifetime around 1.5 ns seen at 800 nm and 810 nm excitation wavelength visible in keratinocytes. **Figure 22** shows MPM-FLIM images of Keratinocytes after the siRNA silencing at 780 nm excitation wavelength and fluorescence lifetime distribution histograms obtained from both channels (blue 445/60 nm and red 580/150 nm). As seen in the figure, MPM-FLIM image of non-targeting siRNA silencing samples (NT siRNA, the control sample) resulted in green color (longer lifetime). Whereas MPM-FLIM images of siRNA silencing of both KRT5 and KRT14 silenced samples are in orange color (short lifetime) when excited at 780 nm. Moreover, in the fluorescence lifetime histograms of both KRT5 and KRT14 proteins samples the 1.5 ns lifetime vanished as compared to the control keratinocytes sample (NT siRNA). Thus, the observed lifetime around 1.5 ns at the excitation wavelength 800 and 810 nm may be corresponding to keratin.

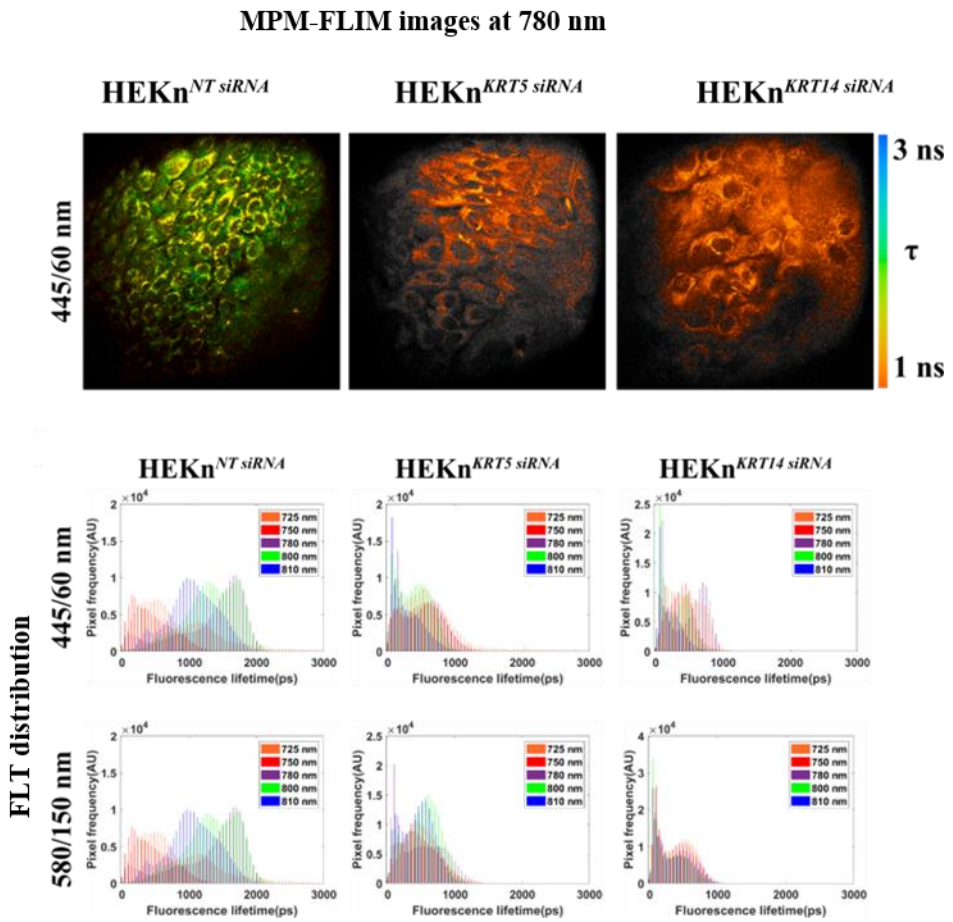

Figure 22. *Effect of keratin 5 and keratin 14 silencing with siRNA on fluorescence lifetime distribution in keratinocytes. MPM-FLIM images of HEKn$^{NT\ siRNA}$, HEKn$^{KRT5\ siRNA}$ and HEKn$^{KRT14\ siRNA}$ obtained from blue channel (445/60 nm) when excited at 780 nm along with fluorescence lifetime distribution histograms recorded from both blue (445/60 nm) and red (580/150 nm) channel at different excitation wavelength (725 nm, 750 nm, 780 nm, 800 nm and 810 nm). Field of view: ~ 350 x 350 µm. False-color scale fluorescence lifetime ranging from 1 to 3 ns, 256-time channels. Brightness and contrast have been adjusted for clarity.*

These findings are verified with complementary different biochemical analysis such as western blotting and immunofluorescent staining of keratin 5 and keratin 14 proteins in the keratinocytes (See paper 4). Thus, the analysis of MPM-FLIM images obtained from cellular autofluorescence is complex and challenging. The contribution from other potential cellular fluorophores should be considered not just NADH and FAD. This characterization study exposes the challenges in interpreting the FLIM data and bring out the importance of FLIM characterization before using the technique for complex biomedical applications like cellular metabolism.

Chapter 7. Conclusions and Future Outlook

7. Conclusion and Future Outlook

There is a quest for the development of quantitative microscopy techniques to advance the translation biomedical research. Being an optimal non-invasive imaging modality, MPM has a prime role in this evolution, and it has been explored in many areas of science especially for skin research. The overall aim of the Ph.D project was to adopt MPM focusing on quantitative fluorescence techniques such as FCS and FLIM for various biomedical applications. One part of this entire research expedition was method development, by exploring different settings and experimental protocols to solve the instantaneous hurdles. These systematic proceedings aided in the execution of MPM adopting FCS and FLIM for answering distinct biomedical questions more effectively in a quantitative perspective.

In paper 1, a systematic practical guideline for MPM-FCS was developed by performing validation experiments using rhodamine B solutions. Optimal experimental conditions such as concentration, objective lens together with a customized FCS data analysis based on time correlated single photon counting technique. In addition, an inverse relationship of laser power on the measured diffusion time was observed. This inverse relationship is due to the difference in the shape of the excitation volume when laser power is varied. This finding opens up further research to develop a theoretical model to measure precise diffusion constant to extend the applicability of FCS in combination with imaging.

The MPM-FCS methodology developed in paper 1 was applied to measure the diffusion time of Rhodamine B in different water glycerol mixtures of varying viscosity (paper 2). The linear relationship between the diffusion time and viscosity was demonstrated. As a proof of principle, the viscosity of two different collagen gel matrix samples (1 mg/ml and 4 mg/ml) were calculated from the diffusion time-viscosity calibration plot. In addition to that the size of the diffusing molecule can be measured form the viscosity-diffusion time function.

The next phase is to apply MPM-FCS in complex biological samples to measure diffusion parameters of pharmaceutically relevant particles. Cyclodextrins are known to be carrier molecules in drug delivery systems and beneficial in pharmaceutical applications [95]. Recently Rhodamine B isothiocyanate labelled cyclodextrin particles (Cyclolab, Hungary) demonstrated promising results in drug delivery studies in biofilms [96]. These types of studies can be done in complex biological samples (cell culture, biofilms and skin) by measuring the diffusion parameters using MPM-FCS method. In addition to that MPM-FCS can be applied to measure the viscosity at cellular level by the similar approach in paper 2.

7.Conclusion and Future Outlook

To facilitate the expansion of non-invasive optical tools to diagnose melanoma metastasis, MPM-FLIM was employed on sentinel lymph nodes exercised from melanoma patients. Investigations done on melanoma positive and negative lymph nodes reported MPM-FLIM as a potential technique with the abilities to differentiate metastasized and non-metastasized regions of lymph nodes. Up to the best of my knowledge, this was the first study examining the melanoma metastasis in human sentinel tissue by adopting MPM-FLIM. With the elevated morphological contrast MPM-FLIM was capable to provide fluorescence lifetime information from each pixel. Furthermore, MPM-FLIM was adequate to distinguish malignant atypical cells, healthy lymphocytes, blood vessels and erythrocytes in the lymph node.

The investigations focusing on the effect of excitation wavelength on cellular fluorescence in keratinocytes was another steppingstone in the development of MPM-FLIM as a non-invasive label free quantitative microscopy technique. The combination of 2PE excited spectral characterization together with MPM-FLIM in cells and fluorophores in solution forged a standardized mode of approach. It revealed the importance of significant cellular fluorophores other than NADH and FAD such as keratin in imaging keratinocytes. Spectral crosstalk of keratin with NADH and a fluorescence lifetime of 1.5 ns was observed. The results from the complementary biochemical analysis such as western blotting and immunofluorescent staining of keratin proteins in the keratinocytes together with MPM-FLIM data of siRNA silencing of keratin expressions (KRT5 and KRT 14) pointed out the lifetime of 1.5 ns, possibly keratin. These findings suggest that serious attention is required when interpreting the fluorescence lifetime data to apply MPM-FLIM as a non-invasive label-free technique particularly for skin related studies.

As discussed in paper 3 and 4, MPM-FLIM has emerged as a non-invasive label free imaging technique with fluorescence lifetime data at pixel level. To develop MPM-FLIM as a reliable clinical tool for melanoma diagnosis further future research needs to be carried out. MPM-FLIM *ex vivo* studies need to be done on sentinel lymph nodes from melanoma model mice to validate the results obtained from human sentinel lymph nodes extracted from melanoma patients (paper 3). Finally, similar experiments will be done on freshly removed sentinel lymph nodes from melanoma patients. The possibilities of this study were already undertaken during my Ph.D. period. However, it is far from an easy task; both logistical and technical challenges need to be addressed.

7.Conclusion and Future Outlook

Another potential future project is under discussion, which is the application of MPM-FLIM for diagnosing different skin disorders (such as eczema and psoriasis) in combination with reflectance confocal microscopy. The reflectance confocal microscopy has already been used clinically at Sahlgrenska University hospital, Gothenburg, Sweden. By combining novel microscopic techniques, non-invasive, fast and accurate diagnostic procedures can be developed in complementary to the histopathological analysis. A well-structured interdisciplinary team consisting of dermatologists, surgeons, pathologists, and biophotonics specialists are required to translate MPM-FLIM from laboratory to clinic. Biomedical photonics research group (University of Gothenburg, Sweden) is closely working with the dermatology and pathology departments at Sahlgrenska University hospital, Gothenburg, Sweden.

The current experimental MPM set-up can be updated with newly developed lasers with longer tunable range (Mai Tai DeepSea, Spectra Physics, 700-1100 nm) and spectral detectors as in commercial systems (LSM 710 NLO, Carl Zeiss, Germany). This feature will enable to perform MPM-FLIM together with spectral imaging which can be applied to explore the metabolic changes in epidermal differentiation in *in vitro* 3D skin model and ultimately organogenesis. The results from paper 4 revealed the importance of keratin autofluorescence pointing towards the spectral and fluorescence lifetime crosstalk with NADH. Thus, more fundamental studies focusing on demonstrating the changes in fluorescence lifetime of NADH in free and bound form are required as such type of molecular level explorations are scarce. This will help to interpret the MPM-FLIM data in a better way. Altogether, MPM-FLIM can be developed as a powerful biomedical imaging modality for both research and clinical purpose in the future.

In conclusion, the work presented in this thesis made it one step closer to utilize the quantitative aspects of MPM focusing on FCS and FLIM. Still this cycle needs to continue emphasizing on understanding the fundamental principles which is required in order to translate the techniques clinically in the future.

Chapter 8. Acknowledgements

8. Acknowledgements

I would like to thank everyone who helped me to complete my Ph.D. journey.

First, I express my sincere gratitude to my supervisor, Marica B. Ericson, for moulding me from a student to a researcher. You were always there for discussion, being optimistic, flashing light at every step of mine with your immense knowledge and expertise. This thesis would have not been possible without your guidance. Thanks for the love and support at my tough times!

Many thanks to my co-supervisor, Jonas Enger, for your guidance and I really enjoyed discussing optics with you. Thanks for taking your time providing input in writing the thesis. You are such a nice person to work with! Thanks to Richard Neutze for all the inputs and suggestions throughout these years and for being my examiner.

I want to thank all the past and present members of the biomedical photonics group: Johan Borglin, thanks for your work in the laser lab during your Ph.D. and the suggestions when I started my work here. Hanna Thomsen, thanks for the discussions, inputs to my work and helping me to learn the biofilm culturing. It was great to work with you. Monika, I am grateful to work with you. It was fun to plan and do MPM-FLIM experiments with you. Thanks for the data discussions, inputs, talks and being a good friend and colleague. Looking forward to seeing your research progress in the future. I want to thank all the bachelor and master students worked in the group during these years to create a good environment. Thank you Rasmus Björk for contributing to the FCS project and working in the laser lab. Thanks to Andreas Schreiber and Bushra Annam Ali Butt for performing spectroscopic studies of NADH. Thanks to Maria Gunnarsson for being a good colleague for a brief period.

Despoina Kantere, I am glad to work with you for melanoma studies and teaching me the medical, dermatological aspects. I would like to thank all the members of the research group at the Department of Dermatology and Pathology, Sahlgrenska University Hospital Gothenburg, for the support. Thanks to all the external collaborators (Cyclolab, Hungary and Laboratory of molecular materials, Linköping University, Sweden) for providing the samples and being supportive.

I want to thank Maria Smedh, Julia Fernandez-Rodriguez and other staff at center for cellular imaging for providing the advanced microscopy experience and sharing the knowledge. Many thanks to Dag Hanstorp, Department of Physics for introducing me to research and being supportive. Thanks to Julie Grantham for sharing the biological knowledge for MPM-FLIM

8.Acknowledgements

studies. Thanks to Patrik Frihlén, Alexander Gunnarsson from Azpect AB for the technical support for Tsunami laser throughout these years. Thank you, Martin Sveningsson, for LABVIEW support.

Thanks to all the people on floor 8 for being friendly and creating a nice working environment. Thanks to all the teaching and administrative staff at the department for the support.

Thanks, Swedish Research Council, the Carl Trygger foundation, and Governmental Funding under the ALF Agreement for funding this research. I want to thank all the other funding agencies for providing the travel stipends during these years.

Thanks to all my friends around the world especially Kevin for the love, support and being in my life. Finally biggest thanks to my family, I do not know how to express my gratitude. Appa, I hope that you are proud of me now and blessing me from heaven. Amma and my big brother, thanks for being in my life and I do not know what my life would have been without you both. My beloved husband and love, Iypu; you are the best thing that happened to me in these years. Thanks for being my life.

Chapter 9. Bibliography

9. Bibliography

1. Bennett, J.A., *The social history of the microscope.* Journal of Microscopy, 1989. **155**(3): p. 267-280.

2. Meyer-Arendt, J.R., *Optical Instrumentation for the Biologist: Microscopy.* Applied Optics, 1965. **4**(1): p. 1-9.

3. Barnard, J.E., *Microscopy with Ultra-violet Light.* Nature, 1920. **106**: p. 378.

4. Hooke, R., J. Allestry, and J. Martyn, *Micrographia, or, Some physiological descriptions of minute bodies made by magnifying glasses :with observations and inquiries thereupon*. 1665, London :: Printed by Jo. Martyn and Ja. Allestry, printers to the Royal Society.

5. Wollman, A.J.M., et al., *From Animaculum to single molecules: 300 years of the light microscope.* Open Biology, 2015. **5**(4): p. 150019.

6. Airy, G.B., *On the Diffraction of an Object-glass with Circular Aperture.* Transactions of the Cambridge Philosophical Society, 1835. **5**: p. 283.

7. Abbe, E., *Beiträge zur Theorie des Mikroskops und der mikroskopischen Wahrnehmung.* Archiv für mikroskopische Anatomie, 1873. **9**(1): p. 413-418.

8. Rayleigh, *XXXI. Investigations in optics, with special reference to the spectroscope.* The London, Edinburgh, and Dublin Philosophical Magazine and Journal of Science, 1879. **8**(49): p. 261-274.

9. Semwogerere, D., E.R.J.E.o.b. Weeks, and b. engineering, *Confocal microscopy.* 2005. **23**: p. 1-10.

10. Hell, S.W. and J. Wichmann, *Breaking the diffraction resolution limit by stimulated emission: stimulated-emission-depletion fluorescence microscopy.* Optics Letters, 1994. **19**(11): p. 780-782.

11. Denk, W., J.H. Strickler, and W.W. Webb, *Two-photon laser scanning fluorescence microscopy.* Science, 1990. **248**(4951): p. 73-6.

12. Zipfel, W., R. Williams, and W. Webb, *Zipfel WR, Williams RM, Webb WWNonlinear magic: multiphoton microscopy in the biosciences. Nat Biotechnol 21:1369-1377*. Vol. 21. 2003. 1369-77.

13. Konig, K., *Multiphoton microscopy in life sciences.* Journal of Microscopy, 2000. **200**(2): p. 83-104.

14. Paoli, J., et al., *Multiphoton Laser Scanning Microscopy on Non-Melanoma Skin Cancer: Morphologic Features for Future Non-Invasive Diagnostics.* Journal of Investigative Dermatology, 2008. **128**(5): p. 1248-1255.

15. Balu, M., et al., *In Vivo Multiphoton Microscopy of Basal Cell Carcinoma.* JAMA dermatology, 2015. **151**(10): p. 1068-1074.

9.Bibliography

16. Zipfel, W.R., R.M. Williams, and W.W. Webb, *Nonlinear magic: Multiphoton microscopy in the biosciences.* Nature Biotechnology, 2003. **21**(11): p. 1369-1377.

17. Williams, R.M., W.R. Zipfel, and W.W. Webb, *Multiphoton microscopy in biological research.* Current Opinion in Chemical Biology, 2001. **5**(5): p. 603-608.

18. Hoover, E.E. and J.A. Squier, *Advances in multiphoton microscopy technology*. Nature photonics, 2013. **7**(2): p. 93-101.

19. König, K., T. Baldeweck, and M. Balu, *Multiphoton Microscopy and Fluorescence Lifetime Imaging : Applications in Biology and Medicine*. 2018, Berlin, Germany: De Gruyter.

20. Haustein, E. and P. Schwille, *Fluorescence Correlation Spectroscopy: Novel Variations of an Established Technique.* Annual Review of Biophysics and Biomolecular Structure, 2007. **36**(1): p. 151-169.

21. Lakowicz, J.R., et al., *Fluorescence lifetime imaging.* Analytical Biochemistry, 1992. **202**(2): p. 316-330.

22. Chang, C., D. Sud, and M. Mycek, *Fluorescence Lifetime Imaging Microscopy,* in *Methods in Cell Biology*. 2007. p. 495-524.

23. Magde, D., E.L. Elson, and W.W. Webb, *Fluorescence correlation spectroscopy. II. An experimental realization.* Biopolymers, 1974. **13**(1): p. 29-61.

24. Elson, E.L. and D. Magde, *Fluorescence correlation spectroscopy. I. Conceptual basis and theory.* Biopolymers, 1974. **13**(1): p. 1-27.

25. Aragón, S.R. and R. Pecora, *Fluorescence correlation spectroscopy and Brownian rotational diffusion.* Biopolymers, 1975. **14**(1): p. 119-137.

26. Webb, W.W., *Applications of Fluorescence Correlation Spectroscopy.* Quarterly Reviews of Biophysics, 1976. **9**(1): p. 49-68.

27. Aragón, S.R. and R. Pecora, *Fluorescence correlation spectroscopy as a probe of molecular dynamics.* The Journal of Chemical Physics, 1976. **64**(4): p. 1791-1803.

28. Abaci, H.E., et al., *Next generation human skin constructs as advanced tools for drug development.* Exp Biol Med (Maywood), 2017. **242**(17): p. 1657-1668.

29. Pappinen, S., et al., *Organotypic cell cultures and two-photon imaging: tools for in vitro and in vivo assessment of percutaneous drug delivery and skin toxicity.* J Control Release, 2012. **161**(2): p. 656-67.

30. Lakowicz, J.R., *Principles of fluorescence spectroscopy*. 3rd ed. 2006: Springer. 1-954.

31. Pawley, J., *Handbook of biological confocal microscopy*. Vol. 236. 2006: Springer Science & Business Media.

32. Göppert-Mayer, M., *Über Elementarakte mit zwei Quantensprüngen.* Annalen der Physik, 1931. **401**(3): p. 273-294.

33. Kirejev, V., et al., *Multiphoton microscopy. a powerful tool in skin research and topical drug delivery science.* Journal of Drug Delivery Science and Technology, 2012. **22**(3): p. 250-259.

34. Helmchen, F. and W. Denk, *Deep tissue two-photon microscopy.* Nature Methods, 2005. **2**: p. 932.

35. WANG, B.-G., K. KÖNIG, and K.-J. HALBHUBER, *Two-photon microscopy of deep intravital tissues and its merits in clinical research.* Journal of Microscopy, 2010. **238**(1): p. 1-20.

36. Masters, B.R., P.T. So, and E. Gratton, *Multiphoton excitation fluorescence microscopy and spectroscopy of in vivo human skin.* Biophysical Journal, 1997. **72**(6): p. 2405-2412.

37. Ericson, M.B., et al., *Two-photon laser-scanning fluorescence microscopy applied for studies of human skin.* Journal of Biophotonics, 2008. **1**(4): p. 320-330.

38. Levene, M.J., et al., *In Vivo Multiphoton Microscopy of Deep Brain Tissue.* Journal of Neurophysiology, 2004. **91**(4): p. 1908-1912.

39. Horton, N.G., et al., *In vivo three-photon microscopy of subcortical structures within an intact mouse brain.* Nature Photonics, 2013. **7**(3): p. 205-209.

40. Bird, D.K., et al., *Metabolic Mapping of MCF10A Human Breast Cells via Multiphoton Fluorescence Lifetime Imaging of the Coenzyme NADH.* Cancer Research, 2005. **65**(19): p. 8766-8773.

41. Provenzano, P.P., K.W. Eliceiri, and P.J. Keely, *Multiphoton microscopy and fluorescence lifetime imaging microscopy (FLIM) to monitor metastasis and the tumor microenvironment.* Clinical & Experimental Metastasis, 2009. **26**(4): p. 357-370.

42. Blacker, T.S., et al., *Separating NADH and NADPH fluorescence in live cells and tissues using FLIM.* Nature Communications, 2014. **5**(1): p. 3936.

43. Skala, M.C., et al., *In vivo multiphoton fluorescence lifetime imaging of protein-bound and free nicotinamide adenine dinucleotide in normal and precancerous epithelia.* Journal of biomedical optics, 2007. **12**(2): p. 024014-024014.

44. Lakowicz, J.R., et al., *Fluorescence lifetime imaging of free and protein-bound NADH.* Proceedings of the National Academy of Sciences of the United States of America, 1992. **89**(4): p. 1271-1275.

45. Chen, Y., J.D. Mills, and A. Periasamy, *Protein localization in living cells and tissues using FRET and FLIM.* Differentiation, 2003. **71**(9): p. 528-541.

46. Kumar, S., et al., *FLIM FRET Technology for Drug Discovery: Automated Multiwell-Plate High-Content Analysis, Multiplexed Readouts and Application in Situ.* 2011. **12**(3): p. 609-626.

47. BECKER, W., *Fluorescence lifetime imaging – techniques and applications.* Journal of Microscopy, 2012. **247**(2): p. 119-136.

9.Bibliography

48. Becker, W., *The bh TCSPC Handbook*. 8th ed. 2019, Berlin, Germany: Becker & Hickel. 1-968.

49. Becker, W., *Advanced time-correlated single photon counting techniques*, in *Springer Series in Chemical Physics*. 2005. p. I-387.

50. O'Connor, D., *Time-correlated single photon counting*. 2012: London, Academic Press.

51. Birch, D.J. and R.E. Imhof, *Time-domain fluorescence spectroscopy using time-correlated single-photon counting*, in *Topics in fluorescence spectroscopy*. 2002, Springer. p. 1-95.

52. Becker, W., *Advanced time-correlated single photon counting techniques*. Vol. 81. 2005: Springer Science & Business Media.

53. Magde, D., E. Elson, and W.W. Webb, *Thermodynamic fluctuations in a reacting system measurement by fluorescence correlation spectroscopy.* Physical Review Letters, 1972. **29**(11): p. 705-708.

54. Schwille, P., *Fluorescence correlation spectroscopy and its potential for intracellular applications.* Cell Biochemistry and Biophysics, 2001. **34**(3): p. 383-408.

55. Wachsmuth, M., W. Waldeck, and J. Langowski, *Anomalous diffusion of fluorescent probes inside living cell nuclei investigated by spatially-resolved fluorescence correlation spectroscopy11Edited by W. Baumeister.* Journal of Molecular Biology, 2000. **298**(4): p. 677-689.

56. Hess, S.T., et al., *Biological and Chemical Applications of Fluorescence Correlation Spectroscopy: A Review.* Biochemistry, 2002. **41**(3): p. 697-705.

57. Schwille, P., J. Korlach, and W.W. Webb, *Fluorescence correlation spectroscopy with single-molecule sensitivity on cell and model membranes.* Cytometry, 1999. **36**(3): p. 176-182.

58. Böhmer, M., et al., *Time-resolved fluorescence correlation spectroscopy.* Chemical Physics Letters, 2002. **353**(5): p. 439-445.

59. Stock, R.S. and W.H. Ray, *Interpretation of photon correlation spectroscopy data: A comparison of analysis methods.* Journal of Polymer Science: Polymer Physics Edition, 1985. **23**(7): p. 1393-1447.

60. Prausnitz, M.R. and R. Langer, *Transdermal drug delivery.* Nature biotechnology, 2008. **26**(11): p. 1261-1268.

61. Brown, M.B., et al., *Dermal and Transdermal Drug Delivery Systems: Current and Future Prospects.* Drug Delivery, 2006. **13**(3): p. 175-187.

62. Esteva, A., et al., *Dermatologist-level classification of skin cancer with deep neural networks.* Nature, 2017. **542**(7639): p. 115-118.

63. Groeber, F., et al., *Skin tissue engineering — In vivo and in vitro applications.* Advanced Drug Delivery Reviews, 2011. **63**(4): p. 352-366.

64. Skardal, A., T. Shupe, and A.J.D.d.t. Atala, *Organoid-on-a-chip and body-on-a-chip systems for drug screening and disease modeling.* Drug discovery today, 2016. **21**(9): p. 1399-1411.

65. Bhatia, S.N. and D.E.J.N.b. Ingber, *Microfluidic organs-on-chips.* Nature biotechnology, 2014. **32**(8): p. 760-772.

66. Schenke-Layland, K. and R.M. Nerem, *In vitro human tissue models — moving towards personalized regenerative medicine.* Advanced Drug Delivery Reviews, 2011. **63**(4): p. 195-196.

67. Huang, S., A.A. Heikal, and W.W. Webb, *Two-Photon Fluorescence Spectroscopy and Microscopy of NAD(P)H and Flavoprotein.* Biophysical Journal, 2002. **82**(5): p. 2811-2825.

68. Breunig, H.G., H. Studier, and K. König, *Multiphoton excitation characteristics of cellular fluorophores of human skin in vivo.* Optics Express, 2010. **18**(8): p. 7857-7871.

69. Wang, X.F., et al., *Fluorescence Lifetime Imaging Microscopy (FLIM): Instrumentation and Applications.* Critical Reviews in Analytical Chemistry, 1992. **23**(5): p. 369-395.

70. Scott, T.G., et al., *Synthetic spectroscopic models related to coenzymes and base pairs. V. Emission properties of NADH. Studies of fluorescence lifetimes and quantum efficiencies of NADH, AcPyADH, [reduced acetylpyridineadenine dinucleotide] and simplified synthetic models.* Journal of the American Chemical Society, 1970. **92**(3): p. 687-695.

71. Cao, R., H. Wallrabe, and A. Periasamy, *Multiphoton FLIM imaging of NAD(P)H and FAD with one excitation wavelength.* 2020. Journal of Biomedical Optics(1): p. 014510.

72. Ehlers, A., et al., *Multiphoton fluorescence lifetime imaging of human hair*. 2007. **70**(2): p. 154-161.

73. Perera E, Gnaneswaran N, Jennens R, Sinclair R. *Malignant melanoma*. Healthcare; 2014: Multidisciplinary Digital Publishing Institute; 2014. p. 1-19.

74. Karimkhani, C., et al., *The global burden of melanoma: results from the Global Burden of Disease Study 2015.* British Journal of Dermatology, 2017. **177**(1): p. 134-140.

75. Markovic, S.N., et al. *Malignant melanoma in the 21st century, part 1: epidemiology, risk factors, screening, prevention, and diagnosis*. in *Mayo Clinic Proceedings*. 2007. Elsevier.

76. Rigel, D.S. and J.A. Carucci, *Malignant melanoma: Prevention, early detection, and treatment in the 21st century.* CA: A Cancer Journal for Clinicians, 2000. **50**(4): p. 215-236.

77. Erdei, E. and S.M. Torres, *A new understanding in the epidemiology of melanoma.* Expert Review of Anticancer Therapy, 2010. **10**(11): p. 1811-1823.

9.Bibliography

78. Atallah, E. and L.J.C.t.o.i.o. Flaherty, *Treatment of metastatic malignant melanoma.* Current treatment options in oncology, 2005. **6**(3): p. 185-193.

79. Amersi, F. and D.L. Morton, *The role of sentinel lymph node biopsy in the management of melanoma.* Advances in surgery, 2007. **41**: p. 241-256.

80. Nathanson, S.D., R. Shah, and K. Rosso, *Sentinel lymph node metastases in cancer: Causes, detection and their role in disease progression.* Seminars in Cell & Developmental Biology, 2015. **38**: p. 106-116.

81. Wilke, L.G., et al., *Surgical Complications Associated With Sentinel Lymph Node Biopsy: Results From a Prospective International Cooperative Group Trial.* Annals of Surgical Oncology, 2006. **13**(4): p. 491-500.

82. Wrightson, W.R., et al., *Complications Associated With Sentinel Lymph Node Biopsy for Melanoma.* Annals of Surgical Oncology, 2003. **10**(6): p. 676-680.

83. James, J., J. Enger, and M.B. Ericson, *Fluorescence Correlation Spectroscopy Combined with Multiphoton Laser Scanning Microscopy—A Practical Guideline.* Applied Sciences, 2021. **11**(5): p. 2122.

84. Brand, L., et al., *Single-Molecule Identification of Coumarin-120 by Time-Resolved Fluorescence Detection: Comparison of One- and Two-Photon Excitation in Solution.* The Journal of Physical Chemistry A, 1997. **101**(24): p. 4313-4321.

85. Miller, C.C. and J. Walker, *The Stokes-Einstein law for diffusion in solution.* 1924. **106**(740): p. 724-749.

86. Magde, D., E. Elson, and W.W. Webb, *Thermodynamic Fluctuations in a Reacting System---Measurement by Fluorescence Correlation Spectroscopy.* Physical Review Letters, 1972. **29**(11): p. 705-708.

87. Berland, K. and G. Shen, *Excitation saturation in two-photon fluorescence correlation spectroscopy.* Applied optics, 2003. **42**(27): p. 5566-5576.

88. Hess, S.T. and W.W. Webb, *Focal Volume Optics and Experimental Artifacts in Confocal Fluorescence Correlation Spectroscopy.* Biophysical Journal, 2002. **83**(4): p. 2300-2317.

89. Petrášek, Z. and P. Schwille, *Photobleaching in Two-Photon Scanning Fluorescence Correlation Spectroscopy.* ChemPhysChem, 2008. **9**(1): p. 147-158.

90. Fick, A., *V. On liquid diffusion.* The London, Edinburgh, and Dublin Philosophical Magazine and Journal of Science, 1855. **10**(63): p. 30-39.

91. Gendron, P.O., F. Avaltroni, and K.J. Wilkinson, *Diffusion coefficients of several rhodamine derivatives as determined by pulsed field gradient-nuclear magnetic resonance and fluorescence correlation spectroscopy.* J Fluoresc, 2008. **18**(6): p. 1093-101.

9.Bibliography

92. Porter, G., P.J. Sadkowski, and C.J. Tredwell, *Picosecond rotational diffusion in kinetic and steady state fluorescence spectroscopy.* Chemical Physics Letters, 1977. **49**(3): p. 416-420.

93. James, J., et al., *Report on fluorescence lifetime imaging using multiphoton laser scanning microscopy targeting sentinel lymph node diagnostics.* 2020. Journal of Biomedical Optics(7): p. 071204.

94. Georgakoudi, I. and K.P. Quinn, *Optical Imaging Using Endogenous Contrast to Assess Metabolic State.* Annual Review of Biomedical Engineering, 2012. **14**(1): p. 351-367.

95. Loftsson, T. and D. Duchêne, *Cyclodextrins and their pharmaceutical applications.* International Journal of Pharmaceutics, 2007. **329**(1): p. 1-11.

96. Thomsen, H., et al., *Delivery of cyclodextrin polymers to bacterial biofilms — An exploratory study using rhodamine labelled cyclodextrins and multiphoton microscopy.* International Journal of Pharmaceutics, 2017. **531**(2): p. 650-657.

Appendix (Matlab Code for FCS analysis)

```
close all
clear
%load raw data file containing the photon arrival time
load FCSdata_Burst1_Phot.txt -ascii
%define the photon arrival time to data variable
data = FCSdata_Burst1_Phot (:,1);
%save the data as a mat file
save('data.mat', 'data');
%define the macro time
Macrotime_Ticks  =  12.5; %ns
%Analysis on the effect of reducing time resolution on the data
timeres = [2E4 2E5];
%figure 1 showing FCS curve in different time resolution
f1 = figure;
set(f1, 'Position', [361 397 1523 701])
ax1 = []; ax2 = [];
meanN = [];
    load data.mat;
    % shift data to start from timetag = 1
    data = data-min(data)+1;
    for i = 1:length(timeres)
        %reduce time resolution and rescale to ns
        datai = round(data*Macrotime_Ticks./timeres(i));
        if min(datai)<1
         datai = datai+1;
        end
        % reduce length of data for faster calculations at initial
trial. This step
         % is not making any difference is time-resolution of data
is decreased. So
         % should be validated.
         idx = find(datai<1E7);
         datai = datai(1:max(idx));

         % Create Photon-times array
         Nt = hist(datai,max(datai));
         Ft = Nt;
         dFt = Nt-mean(Nt);
         meanN = [meanN mean(Nt)];
         %dFt = dFt./mean(Nt); %normalisation

        %Compute autocorrelation
        %Gtau = xcorr(Ft);
        %Gtau = Gtau(length(Ft):length(Gtau));
        Gtau = xcorr(dFt);
        Gtau = Gtau(length(dFt):length(Gtau));
        x = 1:length(Ft);
        x = x*timeres(i); %*Macrotime_Ticks;
        Gtau = Gtau.*(length(x)/sum(Ft)^2); %Normalisation

        if i==1
        Data = [x; Gtau];
        end
```

```
      %subplot(2,5,i+5)
      ax =  subplot(3,4,i);
      ax1 = [ax1 ax];
      semilogx(x, Gtau); hold on
      title(strcat('Time res. ', num2str(timeres(i)), ' ns'))
      xlim = get(ax, 'Xlim');
      set(ax, 'Xlim',  [5*timeres(i) max(xlim)])
      ax = subplot(3,4,i+4);
      ax2 = [ax2 ax];
      plot(dFt), hold on
       title('RhB')
     end
% Parameters for diffusion model fit
G0 = 0.3;%set the value manually by observing figure 1
% xv = -6:0.5:1; tau = 10.^xv;
tauD = 0.0065E7; %set the value manually by observing figure 1
% tau = tau*1E9; tauD = tauD*1E9; % rescale to ns
a = 1; % this can be othen than 1 if the fitting is not good
% Gtau_fit = G0./((1+tau/tauD).*sqrt(1+a^2*(tau/tauD)));
% %Gtau_simple = G0./(1+(tau/tauD));
% Gtau_simple = G0./(1+tau/tauD); %.*exp(-tau/tauD).^2;
%figure main FCS curve
f2 = figure;
set(f2, 'Position', [744 630 1.0322e+03 420])
    data = Data;
    tau = data(1,:);
    Gtau_simple = G0./(1+(tau/tauD));
    Gtau_fit = G0./((1+tau/tauD).*sqrt(1+a^2*(tau/tauD)));
    semilogx(data(1,:),data(2,:)); hold on
    semilogx(tau, Gtau_simple, 'r')
    semilogx(tau, Gtau_fit, 'r:')
    ax = gca;
    set(ax, 'XLim', [5E4 1E10])
    set(ax, 'YLim', [-0.02 0.2])
    xlabel('\tau (ns)')
    ylabel('G(\tau)')
    lg = legend('FCS Data', strcat('G simple, \tau_D =',
num2str(tauD/1E6), ' ms'), 'G fit ext');
    set(lg, 'Location', 'Northeast');
    ax = gca;
    set(f2, 'Color', [1 1 1])
    set(ax,'FontSize',12,'FontWeight','bold');
    box on
    %Figure FCS curve in linear scale
    f3 = figure;
    plot(data(1,:), data(2,:)); hold on
    plot(tau, Gtau_simple, 'r')
    plot(tau, Gtau_fit, 'r:')
    ax = gca;
    set(ax, 'XLim', [1E5 1E10])
    xlabel('\tau (ns)')
    ylabel('G(\tau)')
    ax = gca;
    set(f3, 'Color', [1 1 1])
    set(ax,'FontSize',12,'FontWeight','bold');
    box on
```